Conductivity Imaging and Generalized Radon Transform: A Review

Chapter · June 2010

Archontis Giannakidis
Royal Brompton and Harefield NHS Foundation Trust

Comp. by: pg1384Alex, Monica Stage: Proof ChapterID: 0001157249AIEP978-0-12-381316-9 Date:22/4/10 Time:12:24:27
File Path:\\pchns1002z\WOMAT\Production\PRODENV\0000000001\0000018453\0000000016\0001157249.3d
Acronym:AIEP Volume:16204

Chapter 4

Conductivity Imaging and Generalized Radon Transform: A Review

Archontis Giannakidis* and **Maria Petrou**†

Contents

* Faculty of Engineering and Physical Sciences, University of Surrey, Guildford, UK
† Department of Electrical and Electronic Engineering, Imperial College, London, UK

Advances in Imaging and Electron Physics, Volume 162, ISSN 1076-5670, DOI: 10.1016/S1076-5670(10)62004-6.

Comp. by: pg1384Alex, Monica Stage: Proof ChapterID: 0001157249AIEP978-0-12-381316-9 Date:22/4/10 Time:12:24:27
File Path:\\pchns1002z\WOMAT\Production\PRODENV\0000000001\0000018453\0000000016\0001157249.3d
Acronym:AIEP Volume:16204

1. INTRODUCTION

Living tissues are electrical conductors because of the movable ions that they contain. However, not all types of organic tissue conduct electricity with the same ease. In the human body, for example, there is a significant variation of conductivity (up to 265:1) among the different tissue types (Geddes & Baker, 1967). Therefore, it should be possible to use conductivity distribution values to extract useful structural and anatomical information about the human body. Furthermore, pathological situations change the normal range of values for tissue conductivity. For example, as early as 1923, Grant (1923) found that at 1 KHz, cerebral gliomas[1] had a conductivity double that of normal tissue. Also, it has been shown that the conductivity in the cerebrum[2] reduces by a factor of 2 during stroke (Hossman, 1971) and by up to 17% during epilepsy (Van Harreveld & Schadé, 1962). Hence, the conductivity distribution inside the human body may also manifest tissue diseases. Finally, the values of the electrical properties of some human organs, such as the heart, lungs, and brain, depend on their functional state (Eyuboglu et al., 1989; Tidswell et al., 2001a; Witsoe & Kinnen, 1967). As a consequence, the reconstruction of the conductivity distribution also may be used to distinguish various physiological conditions of the human organs.

The noninvasive technique that exploits the phenomena described above by determining the internal conductivity profile of the human body is called electrical impedance tomography (EIT). This name was agreed on at the First European Community Workshop on Electrical Impedance Tomography — Applied Potential Tomography in Sheffield in 1986 (Bayford, 2006). The term impedance is derived from the fact that human tissue is not purely conductive. Many tissues also have a capacitive reactance; therefore, it is more correct to speak of impedance of tissue rather than conductivity (resistivity) of tissue. However, it is most common to reconstruct the distribution of the real part of admittivity (i.e., conductivity), as the recovery of permittivity is hindered by parasitic capacitances that create leakage currents (Barber, 1995). In this chapter, we are concerned with the reconstruction of the conductivity distribution only.

To determine the conductivity distribution within the human body without physically probing it, electrical potential differences are applied to the human body through an array of electrodes attached to its surface. The resulting currents flow through the tissue. Subsequently,

[1] A glioma is a type of malignant tumor that starts in the brain or spine. It is called a glioma because it arises in glial cells.

[2] Cerebrum, which means "brain" in Latin, is the nontechnical term for the telencephalon. The telencephalon and the diencephalon (i.e., thalamus and hypothalamus) comprise the forebrain. The cerebrum is the largest part of the brain and the source of intellectual activities.

Comp. by: pg1384Alex, Monica Stage: Proof ChapterID: 0001157249AIEP978-0-12-381316-9 Date:22/4/10 Time:12:24:27
File Path:\\pchns1002z\WOMAT\Production\PRODENV\0000000001\0000018453\0000000016\0001157249.3d
Acronym:AIEP Volume:16204

measurements of the induced voltages are collected using electrodes—different from those used to excite the medium—to reduce the possibility of current leakage (Barber, 1995). Finally, the conductivity distribution is recovered based on this set of measurements and following one of the reconstruction approaches discussed in Section 2.

The excitation current that flows through the human tissue is alternating current in the range from 1 KHz to 2 MHz for all contemporary EIT equipment (Brown, 2003). At lower frequencies, electrode effects and electrical safety considerations are important, whereas at higher frequencies measurement difficulties arise from the effect of stray wiring capacitances (Barber & Brown, 1984). The frequency of the excitation current has a dramatic effect on tissue conductivity (Stuchly & Stuchly, 1980). Other factors such as temperature also have a strong influence on tissue conductivity (Gersing, 1999).

EIT has substantial potential in various applications. Solving the EIT reconstruction problem has many advantages. First, it is a nondestructive and noninvasive imaging tool; therefore; the monitoring process is completely painless. Also, its probes use nonionizing radiation; hence, it is completely safe and harmless and carries no hazards. In addition, an EIT instrument is inexpensive and can be manufactured at the cost of a few thousand pounds (Boone et al., 1994). Furthermore, the equipment is small and portable, and therefore offers the potential for ambulatory monitoring. In general, compared with other imaging modalities, such as X-ray computed tomography (CT) and positron emission tomography (PET), EIT equipment is about a thousand times less expensive and a thousand times smaller (dos Santos & Slutsky, 2005). Another distinct feature of EIT is that it is a rapid technique. Data acquisition and image reconstruction can be fast, and in principle, thousands of images can be obtained per second (Cinel et al., 2007). These advantages make it possible to identify many possible clinical applications, as described in Section 4.

However, despite its advantages, EIT has not yet been established as a routine imaging technique in medicine because the quality of the reconstructed images is poor. The main reasons for poor-quality images are limited spatial resolution due to the limited number of measurements, increased sensitivity of the reconstructed image to voltage measurement errors, reduced sensitivity toward the center of the examined object, and deficiencies of the reconstruction algorithms—for example, the inadequacy in creating an accurate mathematical model of the human body shape.

This chapter is organized as follows. In Section 2 we discuss the reconstruction process in EIT, focusing on the inversion of a generalized Radon transform (GRT). The key problem areas of EIT are analyzed in Section 3. In Section 4 we present the clinical applications of EIT. In Section 5 we present our conclusions and future applications.

Comp. by: pg1384Alex, Monica Stage: Proof ChapterID: 0001157249AIEP978-0-12-381316-9 Date:22/4/10 Time:12:24:27
File Path:\\pchns1002z\WOMAT\Production\PRODENV\0000000001\0000018453\0000000016\0001157249.3d
Acronym:AIEP Volume:16204

2. THE RECONSTRUCTION PROCESS IN EIT

The task of a reconstruction algorithm in EIT is to convert voltage measurements, taken at the boundary of some region, into an image of the spatially varying conductivity distribution within the region. The volume of literature on this inverse problem is huge. We discuss the more frequently used techniques.

2.1. Data-Fitting Methods

One approach traditionally used by researchers to deal with the EIT reconstruction problem is to formulate it as a minimization problem. According to this technique, first used by Yorkey et al. (1987), a functional, which represents the discrepancy between the measured voltages and those computed by a hypothesized conductivity (σ) distribution, is defined and followed by a search for the distribution of σ values that minimizes this functional in the least-squares error (LSE) sense.

The optimization problem is reduced to a system of nonlinear equations (Cheney et al., 1999). Hence, a solution for the conductivity distribution that fits the measurements in an LSE sense can be obtained only by an iterative method. The most efficient numerical technique to perform this least-squares estimation is the Gauss–Newton method (Ortega & Rheinboldt, 1970).

Following this gradient-based method, an initial (usually uniform) estimate of the conductivity distribution is chosen, which is improved iteratively by a quantity obtained by solving a system of linear equations. In order to estimate the conductivity update at each iteration, an approximate Hessian matrix must be inverted. This matrix is positive definite; therefore, the convergence of the iterative method is guaranteed (Yorkey, 1990) as long as a good initial approximation for the conductivity distribution was selected.

The calculation of the approximate Hessian matrix involves the calculation of the complete matrix of partial derivatives of the approximated voltage measurements with respect to conductivity parameters, the Jacobian matrix. Kaipio et al. (2000) present a proof for the differentiability mentioned above. Computationally efficient methods for the calculation of the Jacobian are discussed by Lionheart (2004) and Yorkey (1990).

However, the condition number—the ratio of the maximal to minimal eigenvalue—of the approximate Hessian matrix is typically large — on the order of 10^6 (Yorkey et al., 1987). In addition, the vector of constant terms of the system of linear equations, solved at each iteration to give the conductivity update, depends on the voltage measurements. The combination of these effects results in small voltage measurement errors causing arbitrarily large errors in the conductivity update estimation, or in general, in the least-squares output, when inverting the approximate Hessian matrix. The unstable inversion of the approximate Hessian matrix renders the EIT reconstruction problem, following this approach, ill-conditioned in the Hadamard sense (Hadamard, 1923).

In order to control to some degree the ill-conditioned process, the truncated singular value decomposition has been applied (Tang et al., 2002). However, the most popular strategy to deal with the illconditioning is by using Tikhonov-type regularization methods (Tikhonov & Arsenin, 1977). These methods involve the introduction to the minimization problem of additional information about the quantity to be estimated. Prior information, which is often used in EIT, is related to the positivity (Hua et al., 1991), size (Hua et al., 1991), variation (Cohen-Bacrie et al., 1997), and smoothness properties (Hua et al., 1991) of the solution (i.e., the conductivity distribution). These constraints are incorporated in the reconstruction process in the form of a term of the functional to be minimized. Hence, aside from the mismatch term, the modified functional also consists of a second term, usually called the penalty term, that takes the prior information into account. The role of the regularization term is to penalize solutions that, according to the prior information, are unlikely to happen. The degree to which the prior knowledge affects the solution can be selected. Depending on the prior knowledge about the conductivity distribution, various regularization terms have been constructed and used (Bayford, 2006; Cohen-Bacrie et al., 1997; Hua et al., 1991).

In situations of practical interest—for example, dealing with human organs—the conductivity distribution presents sharp variation. Therefore, it is very challenging to construct regularization terms that incorporate realistic spatial prior information. Much effort has been directed to this construction. Some approaches proposed in the literature include subspace methods using basis constraints (Vauhkonen et al., 1997, 1998) and use of Gaussian anisotropic filters (Borsic et al., 2002). In addition, anatomical information obtained from magnetic resonance imaging (MRI) equipment has been used to construct appropriate regularization operators (Glidewell & Ng, 1997; Kaipio et al., 1999; Vauhkonen et al., 1997). Based on the minimal total variation method (Dobson & Santosa, 1994), which is a distinct optimization method on its own, the total variation could be used to obtain an appropriate and reality-consistent representation of the spatial prior information about the conductivity distribution. However, such a constraint, even though it allows step changes, it results in a nondifferentiable regularization term (Kaipio et al., 2000). Hence, it is not possible to use the Gauss–Newton method because calculation of the Jacobian, which is required for the inversion, also involves (aside from the differentiation of the computed measurements) the differentiation of the regularization term.

In general, some interesting choices of the regularization functional that allow sharp transitions in the conductivity distribution result in nondifferentiable terms (Kaipio et al., 2000; Lionheart, 2004). In such cases, non-smooth optimization methods should be used. However, these methods are computationally expensive (Lionheart, 2004). An alternative suggestion (Kaipio et al., 2000) is the use of a Bayesian approach, which casts the inverse EIT problem in the form of probabilistic inference. However, estimating the whole *a posteriori* probability distribution of the sought conductivity parameters conditioned on the measurements, based as well on prior information, followed by a Markov-chain Monte Carlo integration method to yield the best estimate, is also very time consuming. Therefore, the Bayesian approach is more suitable for geophysics (Tarantola & Valette, 1982) than medicine, or, alternatively, it could be used only as a tool to evaluate the underlying assumptions (Kaipio et al., 2000).

The regularization methods discussed above are effective against EIT instability. However, an important aspect of these methods is that they should produce reasonably accurate reconstructions, even when the prior information used is incompatible with the data (Borsic et al., 2002; Kaipio et al., 1999; Vauhkonen et al., 1998). In this way, the inverse solutions remain unbiased toward the assumed distribution.

2.1.1. The Forward EIT Problem

At each iteration of the reconstruction approach as described, it is necessary to compute the predicted measurements using the current conductivity estimate. At the end of the optimization process, the mismatch measure between predicted and observed measurements falls to a minimum in the LSE sense. The mapping of the interior conductivity distribution into the set of predicted surface voltage measurements, given the current pattern applied to the boundary surface of the object, is achieved by solving the forward EIT problem.

From the inverse problem formulation it becomes clear that errors in the forward solution introduce errors in the reconstructed conductivity profile. Another practical issue related to the iterative reconstruction method is that for convergence to be possible, the predicted voltages must be equal to the measured ones, when the correct conductivity values are used in the forward problem. From the above it is obvious that the accurate solution of the forward EIT problem is a prerequisite for accurate conductivity recovery.

The mathematical modeling of the forward EIT problem is given by Poisson's equation subject to a Neumann boundary condition as follows:

$$\nabla \cdot (\sigma \nabla u) = 0, \text{ in } \Omega \tag{1}$$

$$\sigma \frac{\partial u}{\partial n} = \psi, \text{ on } \partial\Omega, \tag{2}$$

where u denotes the distribution of the electrical potential within (and on the boundary surface $\partial\Omega$ of) the ohmic and isotropic volume of interest Ω, ψ is the density of the low-frequency current applied to $\partial\Omega$, σ is the interior conductivity profile, the symbol ∇ denotes the nabla or del operator,[3] and is the symbol for the dot product of two vectors. Also, $\frac{\partial u}{\partial n}$ is the normal derivative of the scalar electric potential u to $\partial\Omega$—that is, the rate at which u changes in the direction of the outward normal unit on $\partial\Omega$.

Strictly speaking, Eqs. (1) and (2) are correct only for direct current (DC). However, for the range of frequencies of alternating current (AC) at which contemporary EIT systems operate (up to 2 MHz) and the sizes of the objects being imaged, it can be assumed that these equations continue to describe the instantaneous potential distribution within (and on the surface of) the conducting object. Appendix B shows how the quasi-static approximation, described by Eqs. (1) and (2), is obtained from Maxwell's equations. In some situations, where the quasi-static assumption is no longer valid—for example, in the development of EIT systems of larger bandwidth—the implementation of an EIT forward model that is based on the full Maxwell's equations has been proposed (Soni et al., 2006).

The Neumann boundary value problem, described by Eqs. (1) and (2), has a solution up to an additive constant only (Courant & Hilbert, 1968). To obtain a unique solution for u, the special condition prescribed is

$$\int_{\partial\Omega} u\,ds = 0, \tag{3}$$

where ds is the infinitesimal surface element on $\partial\Omega$. This condition is equivalent to choosing a point on $\partial\Omega$ that has zero potential, the reference point or "ground."

In the Neumann boundary condition of Eq. (2), the applied current density ψ is a continuous function on $\partial\Omega$. However, in practice, current is injected through a discrete number of electrodes. To obtain a more accurate model, we must incorporate this discreteness into the forward solver. Hence, the boundary condition of Eq. (2) needs to be modified so that the current density is nonzero at the area of $\partial\Omega$ that corresponds to the current-injecting electrodes and zero at the gaps in between. Similarly, the electrode discreteness necessitates appropriate modification of the special condition in Eq. (3), which describes the choice of "ground." In addition, the continuum model of the forward problem, as described by Eqs. (1)–(3), does not take into account the high conductivity of the electrodes. This effect can be incorporated into the forward solver by imposing the additional constraint

[3] The nabla operator is defined in Cartesian coordinates as $\nabla = \frac{\partial}{\partial x}\hat{\mathbf{x}} + \frac{\partial}{\partial y}\hat{\mathbf{y}} + \frac{\partial}{\partial z}\hat{\mathbf{z}}$, where $\hat{\mathbf{x}}$, $\hat{\mathbf{y}}$, and $\hat{\mathbf{z}}$ form the basis of the system. Its use simplifies the representation of spatial differential operators, such as the gradient and the Laplacian operator of a scalar function and the divergence and the rotation of a vector field, the definitions of which are given in Appendix A.

of constant potential at each electrode. The implementation of these two issues (i.e., discreteness and high conductivity of electrodes) results in the shunt model (Cheney et al., 1999; Cheng et al., 1989; Somersalo et al., 1992). The forward EIT problem, using the shunt model, is no longer a Neumann problem and to guarantee the existence of a solution, the additional constraint of conservation of charge must be imposed.

To decrease further the error from electrode modeling, aside from the two issues discussed above, the electrochemical effect due to the contact between the electrode and the boundary surface, which creates a thin and highly resistive layer, also must be considered in the mathematical formulation of the forward problem. In this case, the constraint of constant potential at each electrode has to be modified to include the surface impedance. The resulting model is called the complete model (Cheney et al., 1999; Cheng et al., 1989; Somersalo et al., 1992). The existence and uniqueness of the solution of the forward EIT problem, using the complete model, has been proven by Somersalo et al. (1992) who also demonstrated the close match-up of the complete model solution with experimental data.

The solution of the elliptic partial differential equation [Eq. (1)] that models the forward EIT problem, subject to the constraints previously mentioned, can be obtained in analytic form only for relatively simple (idealized) geometries and uniform conductivity distributions (Isaacson, 1986; Pidcock et al., 1995a,b). However, when we examine biological organs, in the majority of cases we must deal with nonhomogeneous media and domains of irregular boundary. To avoid errors in the forward solution, an accurate model of the object to be imaged, Ω, is also required.

Closed-form solutions of the forward EIT problem for realistic models of human body do not exist, and numerical methods are required to approximate the solution. Examples of methods that have been used for the solution of the forward EIT problem include the finite difference method (FDM) (Patterson & Zhang, 2003), the finite volume method (FVM) (Dong et al., 2003), the boundary element method (BEM) (Babaeizadeh et al., 2004), and the finite element method (FEM) (Molinari et al., 2001b). The use of FVM is attractive because it satisfies continuity conditions of both the normal component of the current density and the tangential component of the electrical field at the interfaces (Dong et al., 2003). The BEM is very fast and efficient because the unknown potential needs to be solved only for points on the boundaries of the compartments. However, the BEM is suitable only when the object under investigation consists of a set of nested compartments with constant conductivity (Babaeizadeh et al., 2004; Smulders & van Oosterom, 1992). In addition, the boundary conditions, which take into account the accurate electrode modeling, cannot be easily incorporated into the BEM model (Babaeizadeh et al., 2004). The boundary element formulation of the forward EIT problem can be found in (Gonçalves et al., 2003), (Jain et al., 1997), and (de Munck et al., 1997).

The most appropriate numerical method for nonhomogeneous objects of arbitrary shape is the FEM (Brenner & Scott, 1994). In addition, it offers the highest flexibility in terms of application of boundary conditions imposed by electrodes. As a consequence, the FEM is the most widely used tool for solving the elliptic partial differential equation [Eq. (1)]. To solve the forward EIT problem, the FEM uses a system of linear equations to approximate Eq. (1). For this purpose, the object of interest is divided into small elements. The shape of these elements is usually triangular or quadrilateral for the two-dimensional (2D) case, and tetrahedral or hexahedral for the three-dimensional (3D) case. In this way, the continuous forward EIT problem of determining the potential distribution is converted into the problem of the calculation of a finite number of unknowns (of the system), namely, the potential at the discrete nodes of the finite element (FE) mesh. These nodes also include the electrode positions. Hence, after solving the system of equations, the predicted voltage measurements are obtained by subtracting the related node potentials. In practice, by using appropriate interpolation functions and the computed node potentials, one can determine the electric potential throughout the entire domain.

The assembly of the system of linear equations for the FEM is usually based on the variational principle (Tong & Rossettos, 1977). Details about the generation of the FE matrices can be found in (Hua et al., 1993), (Jain et al., 1997), and (Kaipio et al., 2000). Also, to account for the constraints to which Eq. (1) is subject and to incorporate the effects caused by electrodes as discussed above, the system of linear equations is modified appropriately (Hua et al., 1993).

Burnett (1987) has shown that the FEM converges to the true solution of Eq. (1) as the element's size becomes infinitesimal. Hence, the more elements that are used, the higher the accuracy of the solution. However, by increasing the mesh density, the computational complexity and the memory requirements also increase. In general, the solution of the forward EIT problem using the FEM requires the solution of a large system of equations. In addition, mesh generation is time consuming. The forward solution also must be carried out in every step of the iterative reconstruction process, as described in the previous subsection. This repetitive adjustment of the forward solution results in long computational times in the solution of the inverse EIT problem. Despite the large improvements in computing performance and capacitance, time and memory constraints, combined with the drawback that the computation of the mismatch term may be easily misled by measurement and modeling errors, make it difficult to implement the iterative reconstruction method in *in vivo* clinical situations.

Since the matrix of coefficients of the linear system is typically sparse (Molinari et al., 2001b), one strategy to minimize the computation time involves the employment of sparse-system solvers—for example, the conjugate-gradient method (Golub & Van Loan, 1996) and Cholesky factorization (Golub & Van Loan, 1996). In addition, for cases where the conductivity is known to be constant over some subdomain, an attractive method to reduce the computational complexity is the use of a hybrid boundary element and FE method (Hsiao et al., 2000).

Another strategy to make the algorithm faster, without concurrently increasing the size of the associated system matrices, is to use adaptive meshing (Molinari et al., 2001a). This results in high mesh density in areas of sharp field variation and a coarser mesh in areas of gentle field variation. However, the task of mesh optimization is troublesome, especially in the 3D case. To obtain accurate and efficient meshes for the EIT problem, datasets from CT and MRI have been used and segmented (Tizzard et al., 2005). Parallel computing (Blott et al., 2000; Woo et al., 1990) that distributes the workload onto several processors may also be used to facilitate real-time reconstruction.

To circumvent the long computational times, it has also been suggested by Cheney et al. (1990b) to use only one updating step of the iterative Gauss–Newton optimization method described in this section. The resulting method is called the Newton one-step error reconstruction (NOSER) algorithm, which has produced useful ventilation and perfusion images of human subjects (Cheney et al., 1990b, 1999). However, if the initial estimate is not close to the true distribution, the solution obtained by NOSER is of limited accuracy.

2.2. Sensitivity Methods

The manner in which the voltage measurements and the interior conductivity distribution are related in EIT is inherently nonlinear, as dictated by the governing Eq. (1). However, if the deviation of conductivity, $\delta\sigma$, of the constituent parts of the imaged object from a known constant σ value, σ_c, is small, then the measured voltage profile will be $u = U + \delta U$, where δU is the perturbation of the potential profile U, the profile that would have been obtained if all parts of the object had had the same (σ_c) conductivity value. By substituting $\sigma = \sigma_c + \delta\sigma$ and $u = U + \delta U$, Eq. (1) becomes

$$\Delta\delta U = -\frac{1}{\sigma_c}\nabla\cdot(\delta\sigma\nabla U), \tag{4}$$

where Δ denotes the Laplacian operator, and term $\nabla\cdot(\delta\sigma\nabla\delta U)$ has been set to zero, since the perturbations $\delta\sigma$ and δU are small relative to σ_c and U, respectively, and the second-order terms can be neglected. In addition,

$\nabla \cdot \sigma_c \nabla U$ is zero, because U is the solution for uniformity. We may write[4] $\nabla \cdot (\delta\sigma \nabla U) = \nabla\delta\sigma \cdot \nabla U + \delta\sigma \nabla \cdot \nabla U = \nabla\delta\sigma \cdot \nabla U$. Taking this into account, Eq. (4) reduces to

$$\Delta \delta U = -\frac{1}{\sigma_c} \nabla\delta\sigma \cdot \nabla U. \tag{5}$$

Eq. (5) describes a linear relationship between perturbations $\delta\sigma$ (which is the quantity we want to estimate) and δU. Hence, if we apply a current pattern to the object, the process of recovering $\delta\sigma$, given the voltage changes δU, can be represented by a linear operation.

The linear dependency between $\delta\sigma$ and δU allows Eq. (5) to be expressed, in the discrete domain, as the following system of linear equations, in matrix form:

$$\boldsymbol{\delta U} = S\boldsymbol{\delta\sigma}. \tag{6}$$

In the above equation, $\boldsymbol{\delta U}$ is the vector of voltage difference values between the measurements and the voltages that correspond to uniformity in σ. The latter can be obtained by solving Laplace's equation. Also, $\boldsymbol{\delta\sigma}$ is the unknown vector that represents the conductivity distribution and contains image voxel values of conductivity deviation from the known constant value σ_c, and S is the sensitivity matrix. Then, the reconstruction of $\delta\sigma$ requires the solution of the linear system in Eq. (6).

The sensitivity matrix S is constructed by determining the voltage difference in each electrode pair due to a small perturbation of conductivity in each voxel of the domain. Hence, S is obtained by solving the forward problem (described in the previous section). Geselowitz's theorem (Geselowitz, 1971), which gives the relationship between a conductivity perturbation within the examined object and the boundary voltage changes resulting from this perturbation, also has been used for the calculation of S (Kleinermann et al., 1996). For complex geometries, software packages, such as IDEAS[5] (Integrated Design and Engineering Analysis Software), that solve the forward EIT problem may be used to create matrix S (Bayford et al., 2001).

As mentioned in the Introduction, measurements of surface voltage potential can be made only at a limited number of positions, corresponding to electrodes. Therefore, for one applied current pattern, the knowledge of the available surface voltage measurements is insufficient to uniquely determine $\boldsymbol{\delta\sigma}$ to achieve the spatial resolution in the reconstructed image desired in clinical applications because $\boldsymbol{\delta U}$ is smaller

[4] Appendix A provides a list of rules of calculation useful for manipulating this chapter's formulas that involve differential operators of space.

[5] IDEAS is currently owned by Siemens PLM Software, the headquarters of which are in Plano, TX, USA.

than $\boldsymbol{\delta\sigma}$. This results in many possible alternative reconstructions for the given set of data. Hence, the EIT reconstruction process suffers from illconditioning in the Hadamard sense (Hadamard, 1923).

To overcome this source of illconditioning and obtain sufficient information to determine $\boldsymbol{\delta\sigma}$, we apply a complete set of independent current patterns. This allows us to achieve adequate dimensionality for $\boldsymbol{\delta U}$ by assembling this vector from measurements made for all independent current patterns. Since the number of electrodes, through which we inject the current, is finite, only a finite number of independent current patterns can be defined. Given a total number of N_e electrodes, there are at most N_e-3 independent voltage measurements, since potentials at the two current injection electrodes are excluded and an electrode must be used as a reference (Clay & Ferree, 2002). Also, due to the reciprocity theorem (Helmholtz, 1853), for N_e electrodes there are effectively $\frac{N_e}{2}$ independent injection pairs. Considering all injection and measurement pairs gives $N = \frac{N_e}{2}(N_e - 3)$ independent voltage measurements in total. However, even if after stacking the measured voltages for all independent current patterns to form vector $\boldsymbol{\delta U}$, $\boldsymbol{\delta\sigma}$ is still larger than $\boldsymbol{\delta U}$, then the problem remains ill-posed.

The fact that there are usually fewer independent measurements than unknown voxel conductivities is not the only reason for the problem's ill-posedness. Another stability problem of this reconstruction process is related to the issue that S typically has a large condition number. This means that small errors, both random and systematic, on $\boldsymbol{\delta U}$ may translate into large errors in the estimation of $\boldsymbol{\delta\sigma}$, when inverting S.

Up to a degree, we usually treat the two sources of illconditioning by applying constraints and regularization. Two regularization methods commonly used to invert S are the Tikhonov regularization (Jinchuang et al., 2002) and the truncated singular value decomposition (Bagshaw et al., 2003; Kleinermann et al., 1996; Tidswell et al., 2001b). Regarding the latter method, the optimum level of truncation can be determined using sophisticated methods (Xu, 1998). To enhance further the quality of the produced image, Jinchuang et al. (2002) and Wang et al. (2004) have shown that revised regularization should be used by employing an iterative method—for example, Landweber's iteration (Landweber, 1951). This iterative process, designed especially for dealing with ill-posed problems, can be performed offline (Liu et al., 2004; Wang et al., 2004). Hence, the improved images can be obtained in real time.

Other EIT reconstruction approaches that are also suitable when the unknown conductivity distribution of the examined object does not differ significantly from a uniform one are methods based on Calderón's approach (Calderón, 1980; Cheney et al., 1990a; Isaacson & Cheney, 1991; Isaacson & Isaacson, 1989), methods based on moments (Allers &

Comp. by: pg1384Alex, Monica Stage: Proof ChapterID: 0001157249AIEP978-0-12-381316-9 Date:22/4/10 Time:12:24:29
File Path:\\pchns1002z\WOMAT\Production\PRODENV\0000000001\0000018453\0000000016\0001157249.3d
Acronym:AIEP Volume:16204

Santosa, 1991; Connolly & Wall, 1988), and the backprojection method (Barber & Brown, 1985; Santosa & Vogelius, 1990). Hence, these methods also address the linearized inverse problem in EIT.

The development of the backprojection method by Barber & Brown (1985) was motivated by CT, since backprojection forms the basis for most CT reconstruction techniques (Toft, 1996). However, the backprojection process for EIT is generalized to include backprojection along curved lines. In particular, as argued by Santosa & Vogelius (1990), the appropriate backprojection is one in which the normalized value of the counterclockwise tangential derivative of the boundary voltage perturbation gradient, at a point on the boundary, is projected along the equipotential paths (obtained as if the medium were homogeneous with respect to conductivity) ending at that point on the boundary.

The backprojection method can be shown to be strictly equivalent to sensitivity methods, since in backprojection the reconstruction of the unknown normalized conductivity distribution, represented by a vector, can be performed by the multiplication of the vector of normalized voltage measurements with a matrix that represents the reconstruction operator. However, these two methods had a different historical development. In the next section, we describe the backprojection method in some detail.

2.3. Backprojection Reconstruction Method

Let us assume that the region of interest Ω, the conductivity profile of which presents a small deviation $\delta\sigma$ from a known σ value ($\sigma = \sigma_c$), is the unit disk[6] in $\mathbb{R}^2$; that is, $\Omega = \{\boldsymbol{x} \in \mathbb{R}^2 : |\boldsymbol{x}| < 1\}$ (Figure 1). If Ω had uniform

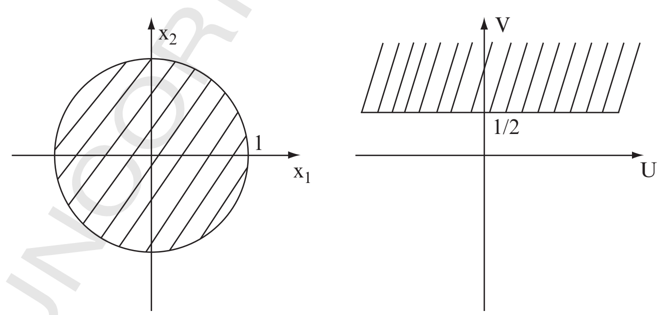

FIGURE 1 The unit disk Ω in the (x_1, x_2) plane and the transformation $(x_1, x_2) \Leftrightarrow (U, V)$.

[6] The treatment of the conductivity reconstruction problem in this section is in two dimensions.

Comp. by: pg1384Alex, Monica Stage: Proof ChapterID: 0001157249AIEP978-0-12-381316-9 Date:22/4/10 Time:12:24:29
File Path:\\pchns1002z\WOMAT\Production\PRODENV\0000000001\0000018453\0000000016\0001157249.3d
Acronym:AIEP Volume:16204

conductivity distribution ($\sigma = \sigma_c$), then the application of a surface current pattern would result in a boundary voltage profile U, which can be estimated by solving Laplace's equation. Hence, the perturbation δU, which is the difference between the measured voltage profile and U when the same current pattern is applied, corresponds to the small perturbation $\delta\sigma$ (of σ), which is the quantity that we want to estimate.

In this treatment, the continuous versions of voltage and conductivity distributions are considered. Therefore, the mathematical model that the backprojection reconstruction method uses to solve the inverse EIT problem is the one described by Poisson's equation [Eq. (1)] subject to the Neumann boundary condition [Eq. (2)]. By applying the perturbation procedure to these equations, similar to the previous section, the linearized problem becomes

$$\Delta\delta U = -\frac{1}{\sigma_c}\nabla\delta\sigma \cdot \nabla U, \text{in } \Omega \tag{7}$$

$$\sigma_c\frac{\partial\delta U}{\partial n} = -\delta\sigma\frac{\partial U}{\partial n}, \text{on } \partial\Omega, \tag{8}$$

where the term $\delta\sigma\frac{\partial(\delta U)}{\partial n}$ was taken equal to zero because it is a second-order term and can be neglected. For simplicity, for the rest of this section we assume that the known constant conductivity value, around which the unknown distribution deviates, is $\sigma_c = 1$.

Let us consider that the excitation current is a dipole located at the boundary location $\boldsymbol{\omega} = (\omega_1, \omega_2)$ ($|\boldsymbol{\omega}| = 1$). Then, it will be $\delta\sigma = 0$ near the dipole (or, equivalently, on the boundary $\partial\Omega$). Taking this into account, the linearized problem reduces to

$$\Delta\delta U = -\frac{1}{\sigma_c} \quad \nabla\delta\sigma \cdot \nabla U, \quad in\ \Omega \tag{9}$$

$$\frac{\partial\delta U}{\partial n} = 0, \text{on } \partial\Omega. \tag{10}$$

To establish the backprojection formula that yields $\delta\sigma$, the linearized problem needs to be transformed into a more convenient coordinate system.

To obtain the new space, we first determine U, which is the solution of Eqs. (1) and (2) for uniformity ($\sigma = \sigma_c = 1$), when the same excitation current (i.e., a dipole located at the boundary location $\boldsymbol{\omega}$) is applied. Then, U solves

$$\Delta U = 0, \text{ in } \Omega \tag{11}$$

$$\frac{\partial U}{\partial n} = -\pi\frac{\partial}{\partial\tau}\delta_{\boldsymbol{\omega}}, \text{ on } \partial\Omega, \tag{12}$$

Comp. by: pg1384Alex, Monica Stage: Proof ChapterID: 0001157249AIEP978-0-12-381316-9 Date:22/4/10 Time:12:24:29
File Path:\\pchns1002z\WOMAT\Production\PRODENV\0000000001\0000018453\0000000016\0001157249.3d
Acronym:AIEP Volume:16204

where $\frac{\partial}{\partial\tau}\delta_{\boldsymbol{\omega}}$ is the counterclockwise tangential derivative of a delta-Dirac function $\delta_{\boldsymbol{\omega}}$, located at the dipole boundary location $\boldsymbol{\omega}$, and the term $-\pi\frac{\partial}{\partial\tau}\delta_{\boldsymbol{\omega}}$ represents the applied current density of the excitation dipole at $\boldsymbol{\omega}$ (Santosa & Vogelius, 1990). Since Ω is the unit disk, the solution to Eqs. (11) and (12) can be obtained (Santosa & Vogelius, 1990) in closed form:

$$U = \frac{x_1^{'}}{x_1^{'2} + x_2^{'2}}, \tag{13}$$

where U is the voltage at any point $\boldsymbol{x} = (x_1, x_2)$ of Ω caused by a uniform conductivity distribution ($\sigma_c = 1$), $x_2{'} = 1 - \boldsymbol{\omega} \cdot \boldsymbol{x}$, and $x_1^{'} = \boldsymbol{\omega}^{\perp} \cdot \boldsymbol{x}$, with $\boldsymbol{\omega}^{\perp} = (-\omega_2, \omega_1)$ denoting the $\frac{\pi}{2}$ rotation of $\boldsymbol{\omega}$ Eq. (13) implies that, for the case of uniform conductivity inside Ω, the equipotentials, represented by curves of constant U, are arcs of circles that originate from dipole positions. Also, it is known that paths of current flow (isocurrents) are orthogonal to equipotentials. Hence, the curves of current flow will also be arcs of circles (including the boundary of the circular region) between the electrodes, perpendicular to equipotentials.

If we define variable V as

$$V \equiv \frac{x_2^{'}}{x_1^{'2} + x_2^{'2}}, \tag{14}$$

where $x_1^{'}$ and $x_2^{'}$ are the same as in Eq. (13), then curves of constant V represent current flow paths, perpendicular to equipotentials.[7]

Then the appropriate transformation for the backprojection formula is the bipolar one, described by Eqs. (13) and (14). By applying this transformation, the linearized problem, described by Eqs. (9) and (10), is converted from the (x_1, x_2) plane into the more convenient rectangular coordinate system (U,V):

$$\Delta\delta U = -\frac{\partial(\delta\sigma)}{\partial U}, \text{ in } P \tag{15}$$

$$\frac{\partial\delta U}{\partial V} = 0, \text{ on } \partial P = \left\{V = \frac{1}{2}\right\}, \tag{16}$$

where the upper half-plane $P = \left\{V > \frac{1}{2}\right\}$ (see Figure 1) is the mapping of unit disk Ω. Also, the circular boundary is mapped onto the line $V = \frac{1}{2}$ (see Figure 1).

Following the coordinate system transformation, the unknown profile $\delta\sigma$ has become a function of U, V, and $\boldsymbol{\omega}$. Similarly, the data $\delta U|_{V=\frac{1}{2}}$ used to

[7] From Eqs. (13) and (14), we may say that variable V is the harmonic conjugate to $-U$ in Ω.

reconstruct $\delta\sigma$ depend on U and $\boldsymbol{\omega}$. However, for a single fixed dipole location, $\boldsymbol{\omega} = \boldsymbol{\omega_0}$, $\delta\sigma$ is a function of U and V, whereas data δU are functions only of U. Following Eqs. (15) and (16), the conductivity increment at any point x of the domain is obtained as follows:

$$\delta\sigma(\boldsymbol{x}(U, \boldsymbol{V}, \boldsymbol{\omega}_0)) = -\frac{\partial}{\partial U}\left(\delta U\Big|_{V=\frac{1}{2}}\right)(U(\boldsymbol{x}, \boldsymbol{\omega}_0), \boldsymbol{\omega}_0). \tag{17}$$

The geometrical interpretation of Eq. (17) is shown in Figure 2. To estimate the conductivity increment $\delta\sigma$ at any point $\boldsymbol{x} = (x_1, x_2)$ of Ω for a fixed dipole location $\boldsymbol{\omega_0}$, we first compute the equipotential $U = s$ that originates at $\boldsymbol{\omega_0}$ and passes through $\boldsymbol{x} = (x_1, x_2)$ by using Eq. (13). This equipotential is the path along which backprojection will occur. Next, we determine the point where this equipotential arc intersects the boundary. This point is the solution (x_1, x_2) that is obtained from Eqs. (13) and (14) for $V = \frac{1}{2}$, $\boldsymbol{\omega} = \boldsymbol{\omega}_0$, and $U = s$. This point is denoted in Figure 2 as $\boldsymbol{x}(s, 1/2, \boldsymbol{\omega_0})$. Finally, the voltage profile at that surface point is backprojected, according to Eq. (17), to yield the required conductivity deviation at point $\boldsymbol{x} = (x_1, x_2)$.

Eq. (17) is valid only for one dipole. When more dipoles are used, then there are many backprojection curves—one for each dipole—and the conductivity increment is given by the average

$$\delta\sigma(\boldsymbol{x}) = \frac{1}{2\pi}\int_{|\boldsymbol{\omega}|=1}\left(\frac{\partial}{\partial U}\delta U\Big|_{V=\frac{1}{2}}\right)(s, \boldsymbol{\omega})\Big|_{s=U(\boldsymbol{x},\boldsymbol{\omega})}(1 - 2V(\boldsymbol{x}, \boldsymbol{\omega}))dS_{\boldsymbol{\omega}}, \tag{18}$$

where V is given by Eq. (14), and the multiplication by $2V(\boldsymbol{x}, \boldsymbol{\omega}) - 1$ in the above equation is performed to compensate (Santosa & Vogelius, 1990)

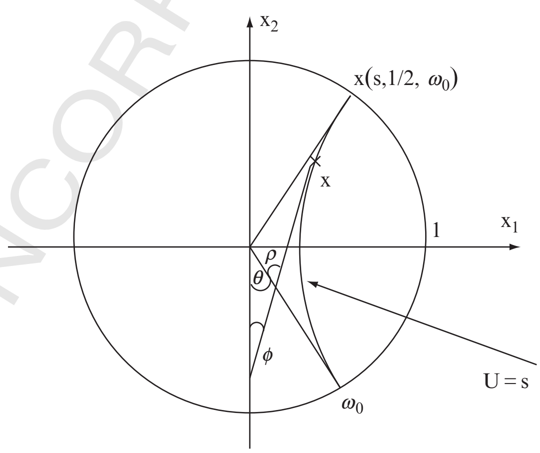

FIGURE 2 The equipotential arc through x and the dipole location $\boldsymbol{\omega_0}$.

for the nonuniform distribution of the angular parameter of the back-projection lines (in the (U, V) space) that pass through the reconstruction point $\boldsymbol{x}$. By using properties of gradient (see (Santosa & Vogelius, 1990) and Appendix A), we have

$$\left(\frac{\partial}{\partial U}\delta U\bigg|_{V=\frac{1}{2}}\right)(s,\boldsymbol{\omega}) = \frac{\nabla\delta U\cdot\nabla U}{|\nabla U|^2}\left(\boldsymbol{x}\left(s,\frac{1}{2},\boldsymbol{\omega}\right),\boldsymbol{\omega}\right), \tag{19}$$

where $\boldsymbol{x}(s, 1/2, \boldsymbol{\omega})$ is a point of the boundary as shown in Figure 2. It is:

$$\begin{aligned}\frac{\nabla\delta U\cdot\nabla U}{|\nabla U|^2}\left(\boldsymbol{x}\left(s,\frac{1}{2},\boldsymbol{\omega}\right),\boldsymbol{\omega}\right) &= \frac{\nabla\delta U\cdot\nabla U}{\nabla U\cdot\nabla U}\left(\boldsymbol{x}\left(s,\frac{1}{2},\boldsymbol{\omega}\right),\boldsymbol{\omega}\right)\\ &= \frac{\nabla\delta U\cdot\dfrac{\nabla U}{|\nabla U|}}{\nabla U\cdot\dfrac{\nabla U}{|\nabla U|}}\left(\boldsymbol{x}\left(s,\frac{1}{2},\boldsymbol{\omega}\right),\boldsymbol{\omega}\right).\end{aligned} \tag{20}$$

Unit vector $\frac{\nabla U}{|\nabla U|}$ lies in the counterclockwise tangential (to the equipotential $U = s$) direction. Hence, both the numerator and the denominator of Eq. (20) represent directional (counterclockwise tangential) derivatives:

$$\frac{\nabla\delta U\cdot\frac{\nabla U}{|\nabla U|}}{\nabla U\cdot\frac{\nabla U}{|\nabla U|}}\left(\boldsymbol{x}\left(s,\frac{1}{2},\boldsymbol{\omega}\right),\boldsymbol{\omega}\right) = \left(\frac{\frac{\partial}{\partial\tau}\delta U}{\frac{\partial}{\partial\tau}U}\right)\left(\boldsymbol{x}\left(s,\frac{1}{2},\boldsymbol{\omega}\right),\boldsymbol{\omega}\right), \tag{21}$$

where $\frac{\partial}{\partial\tau}$ denotes the counterclockwise tangential derivative. Taking Eqs. (19)–(21) into account, Eq. (18) becomes

$$\delta\sigma(\boldsymbol{x}) = \frac{1}{2\pi}\int_{|\boldsymbol{\omega}|=1}\left(\frac{\dfrac{\partial}{\partial\tau}\delta U}{\dfrac{\partial}{\partial\tau}U}\right)\left(\boldsymbol{x}\left(s,\frac{1}{2},\boldsymbol{\omega}\right),\boldsymbol{\omega}\right)\bigg|_{s=U(\boldsymbol{x},\boldsymbol{\omega})}(1-2V(\boldsymbol{x},\boldsymbol{\omega}))dS_{\boldsymbol{\omega}}. \tag{22}$$

Eq. (22) implies that for each current dipole ($\boldsymbol{\omega}$), the measurement[8] that is backprojected to yield the conductivity increment at point $\boldsymbol{x}$ is the one that is taken at the point of the boundary that intersects the equipotential passing through $\boldsymbol{\omega}$ and $\boldsymbol{x}$. Finally, the individual backprojections (measurements) for all dipoles are weighted to account for the nonuniformity of the backprojection paths, and then averaged to give the required conductivity deviation $\delta\sigma$ at point $\boldsymbol{x}$.

[8] By measurement here we mean the normalized value of the counterclockwise tangential derivative of the voltage perturbation gradient.

Comp. by: pg1384Alex, Monica Stage: Proof ChapterID: 0001157249AIEP978-0-12-381316-9 Date:22/4/10 Time:12:24:30
File Path:\\pchns1002z\WOMAT\Production\PRODENV\0000000001\0000018453\0000000016\0001157249.3d
Acronym:AIEP Volume:16204

We must note that the estimated equipotentials, along which the backprojection process takes place to determine $\delta\sigma$, correspond to uniform conductivity. Depending on the degree of nonuniformity, the actual equipotentials deviate from those used above. In fact, the actual paths depend on the actual conductivity to be estimated, which is another manifestation of the nonlinearity of the EIT reconstruction problem. However, because the changes in conductivity for this treatment are assumed to be small, the shape of the equipotentials is not changed significantly. It has been suggested by Barber & Brown (1984) that changes $\delta\sigma$ up to 30% of σ_c are allowable before the use of the backprojection algorithm (or any other linearized reconstruction approach) becomes improper. Another important parameter is that, following the coordinate system transformation previously described, the backprojection process takes place along straight (rather than curved) lines. This fact makes the computation of the coefficients of the reconstruction operator (in the discrete domain) possible (Boone et al., 1997). Next, we show that the backprojection reconstruction process fits within the framework of inverses of GRTs.

2.3.1. Inversion of a Generalized Radon Transform

In this subsection, we show that the linearized inverse EIT problem also can be viewed as a problem in the field of integral geometry. Following this, we demonstrate that an approximate solution to this problem can be obtained by inverting a GRT. The inversion of a GRT is shown to be approximately equivalent to the backprojection process.

The geometry and formulation of the problem in this subsection are similar to the ones used in Section 2.3. Solving Eqs. (15) and (16), with respect to δU, yields

$$\delta U(U, V, \boldsymbol{\omega}) = \int_{-\infty}^{+\infty}\int_{1/2}^{+\infty} G_{(U',V')}(U,V)\,\delta\sigma(U', V', \boldsymbol{\omega})\,dV'\,dU', \tag{23}$$

where

$$G_{(U_0,V_0)}(U,V) = -\frac{1}{4\pi}\left(\frac{U-U_0}{(U-U_0)^2+(V-V_0)^2}+\frac{U-U_0}{(U-U_0)^2+(V+V_0-1)^2}\right), \tag{24}$$

and U_0, V_0 are constants with $V_0 > 1/2$ (Santosa & Vogelius, 1990). Regarding the linearized problem, the integral representation [Eq. (23)] is an integral equation of the unknown function $\delta\sigma$. This equation also models the available data as integrals over geometrical hypersurfaces. Hence, the linearized inverse EIT problem belongs to the field of integral geometry. Equation (23) is also related to a GRT. To see this, let us

Comp. by: pg1384Alex, Monica Stage: Proof ChapterID: 0001157249AIEP978-0-12-381316-9 Date:22/4/10 Time:12:24:30
File Path:\\pchns1002z\WOMAT\Production\PRODENV\0000000001\0000018453\0000000016\0001157249.3d
Acronym:AIEP Volume:16204

first examine the physical interpretation of a GRT and also define such a transformation.

In general, the appearance of the GRT has a simple physical explanation. In some cases, it is impossible to have values of a function directly inside an object of interest, and the only feasible measurements (made over the boundary surface of the object) are integrals of this function. If these integrals are over hyperplanes, then the classical Radon transform applies. Integrals with a weight function over more general hypersurfaces represent the GRT.

The function

$$\phi(\boldsymbol{x}, \boldsymbol{\xi}) = |\boldsymbol{\xi}| U(\boldsymbol{x}, \boldsymbol{\xi}/|\boldsymbol{\xi}|), \ \boldsymbol{x} \in \Omega, \boldsymbol{\xi} \in \mathbb{R}^2 \backslash \{0\}, \tag{25}$$

where U is given by Eq. (13), is a positive homogeneous function of degree 1, and it is also infinitely differentiable in $\Omega \times (\mathbb{R}^2 \backslash \{0\})$. This function defines the family of arcs (parts of circles), which we use as hypersurfaces for the GRT as follows:

$$H_{s,\boldsymbol{\omega}} = \{\boldsymbol{x} \in \Omega : \phi(\boldsymbol{x}, \boldsymbol{\omega}) = s\}, \ s \in \mathbb{R}, |\boldsymbol{\omega}| = 1.$$

We can now define a GRT R for any function g that belongs to the space of functions that are infinitely differentiable in Ω (i.e., $g \in C_0^\infty(\Omega)$) as follows:

$$R(g)(s, \boldsymbol{\omega}) = \int_{H_{s,\boldsymbol{\omega}}} g(\boldsymbol{x}) |\nabla_{\boldsymbol{x}} \phi(\boldsymbol{x}, \boldsymbol{\omega})|^2 d\mu, \tag{26}$$

where $d\mu$ is a measure on each arc $H_{s,\,\boldsymbol{\omega}}$, and the density function was chosen to be equal to $|\nabla_{\boldsymbol{x}}\ \phi\ (\boldsymbol{x},\ \boldsymbol{\omega})|^2$ (Santosa & Vogelius, 1990). To introduce the GRT as defined in Eq. (26) into the linearized inverse EIT problem, we differentiate the integral (23) with respect to U and then estimate the Fourier transform of the result, with respect to s, at value 0. The above calculations yield (Santosa & Vogelius, 1990) the following:

$$-\left(\frac{\frac{\partial}{\partial \tau}\delta U}{\frac{\partial}{\partial \tau} U}\right)\left(\boldsymbol{x}\left(\boldsymbol{s}, \frac{1}{2}, \boldsymbol{\omega}\right), \boldsymbol{\omega}\right) \simeq 2\pi\, K\, R(\delta\sigma)(s, \boldsymbol{\omega}), \tag{27}$$

where $R(\delta\sigma)(s,\ \boldsymbol{\omega})$ is the GRT of the unknown function $\delta\sigma(\boldsymbol{x})$ and K represents convolution with the generalized kernel:

$$k(s) = \frac{1}{2(2\pi)^2} \int_{-\infty}^{+\infty} |r| e^{irs} dr. \tag{28}$$

To invert the GRT of Eq. (27), with the view to yielding $\delta\sigma(\boldsymbol{x})$, let us first introduce a special Fourier integral operator (FIO) F, of a function $h(\boldsymbol{y})$, of the form

Comp. by: pg1384Alex, Monica Stage: Proof ChapterID: 0001157249AIEP978-0-12-381316-9 Date:22/4/10 Time:12:24:31
File Path:\\pchns1002z\WOMAT\Production\PRODENV\0000000001\0000018453\0000000016\0001157249.3d
Acronym:AIEP Volume:16204

$$F(h)(\boldsymbol{y}) \equiv \int_{|\boldsymbol{\omega}|=1} G(\boldsymbol{y}, \boldsymbol{\omega}) dS_{\boldsymbol{\omega}}, \tag{29}$$

where

$$G(\boldsymbol{y}, \boldsymbol{\omega}) = \frac{1}{(2\pi)^2} \int_0^{+\infty} \left(\int_\Omega e^{i\Psi(\boldsymbol{x},\boldsymbol{y},r\boldsymbol{\omega})} A(\boldsymbol{x}, \boldsymbol{y}, r\boldsymbol{\omega}) h(\boldsymbol{x}) d\boldsymbol{x} \right) rdr \tag{30}$$

$$\begin{aligned} \Psi(\boldsymbol{x}, \boldsymbol{y}, \boldsymbol{\xi}) &= \phi(\boldsymbol{x}, \boldsymbol{\xi}) - (\boldsymbol{y}, \boldsymbol{\xi}) \\ A(\boldsymbol{x}, \boldsymbol{y}, \boldsymbol{\xi}) &= \frac{|\nabla_{\boldsymbol{x}} \phi(\boldsymbol{x}, \boldsymbol{\xi}/|\boldsymbol{\xi}|)|^2 \cdot \det\left(\dfrac{\partial^2 \phi(\boldsymbol{y}, \boldsymbol{\xi})}{\partial \boldsymbol{y}_j \partial \boldsymbol{\xi}_k} \right)}{|\nabla_{\boldsymbol{y}} \phi(\boldsymbol{y}, \boldsymbol{\xi}/|\boldsymbol{\xi}|)|^2} \end{aligned} \tag{31}$$

and the function ϕ is given by Eq. (25).

If we consider the even component of $G(\boldsymbol{y}, \boldsymbol{\omega})$ and apply Fubini's theorem (Beylkin, 1984), which gives the conditions under which it is possible to change the order of integration, then FIO F of Eq. (29) can be factored (Beylkin, 1984) in the form

$$F(h)(\boldsymbol{y}) = \boldsymbol{R}^* KR(h)(\boldsymbol{y}), \tag{32}$$

where R and K have been defined above, and operator R^*, which is the dual of R, is defined for any function $k(\boldsymbol{s}, \boldsymbol{\omega})$ as

$$R * (k)(x) \equiv \int_{|w|=1} (2V(x, w) - 1) k(s, w) \bigg|_{s=\phi(x,w)} dS_w, \tag{33}$$

where the weight was chosen to be equal to $(2V(\boldsymbol{x}, \boldsymbol{\omega}) - 1)$ and V is given by Eq. (14) (Santosa & Vogelius, 1990).

FIO F of Eq. (29) is also a pseudodifferential operator and can be represented (Beylkin, 1985) by the sum

$$F(h)(\boldsymbol{y}) = I + T_1 + T_2 + \ldots, \tag{34}$$

where I is the identical operator and operators $T_1, T_1 + T_2, T_1 + T_2 + T_3, \ldots$ belong to increasingly smooth classes of pseudodifferential operators (Beylkin, 1985).[9] Since $T_1 + T_2 + \ldots$ is a compact operator, we may use only the first term in Eq. (34). Then, F approximates the identical operator:

$$F(h)(\boldsymbol{y}) \simeq I \tag{35}$$

[9] To achieve the representation of Eq. (34) for FIO F, the weight function in R^* and the kernel in K have been chosen properly.

The combination of Eqs. (32) and (35) yields

$$R^{*}KR(h)(\boldsymbol{y}) \simeq I. \tag{36}$$

Eq. (36) forms the basis for inverting the GRT of Eq. (27). In addition, due to Eq. (36), operator R^* is also called the generalized backprojection operator.

By applying operator R^* to Eq. (27) and dividing by 2π, we obtain

$$\begin{aligned} &\frac{1}{2\pi}\int_{|\boldsymbol{\omega}|=1}\left(\frac{\frac{\partial}{\partial\tau}\delta U}{\frac{\partial}{\partial\tau}U}\right)\left(\boldsymbol{x}\left(s,\frac{1}{2},\boldsymbol{\omega}\right),\boldsymbol{\omega}\right)\bigg|_{s=U(\boldsymbol{x},\boldsymbol{\omega})}(1-2V(\boldsymbol{x},\boldsymbol{\omega}))dS_{\boldsymbol{\omega}} \\ &\simeq R^{*}KR(\delta\sigma)(\boldsymbol{x}). \end{aligned} \tag{37}$$

By virtue of Eqs. (36) and (37) following approximate[10] solution to the linearized inverse EIT problem is derived as follows:

$$\begin{aligned} &\delta\sigma(\boldsymbol{x}) \simeq \\ &\frac{1}{2\pi}\int_{|\boldsymbol{\omega}|=1}\left(\frac{\frac{\partial}{\partial\omega}\delta U}{\frac{\partial}{\partial\omega}U}\right)\left(\boldsymbol{x}\left(s,\frac{1}{2},\boldsymbol{\omega}\right),\boldsymbol{\omega}\right)\bigg|_{s=U(\boldsymbol{x},\boldsymbol{\omega})}(1-2V(\boldsymbol{x},\boldsymbol{\omega}))dS_{\boldsymbol{\omega}}. \end{aligned} \tag{38}$$

This solution was obtained by inverting the GRT. However, by comparison of Eq. (38) with Eq. (22), it is obvious that the backprojection process in EIT is equivalent to approximately inverting a GRT.

2.4. Other Reconstruction Approaches

Two interesting reconstruction approaches proposed in the literature are the layer-stripping algorithm (Somersalo et al., 1991; Sylvester, 1992) and the $\bar{\partial}$ algorithm (Siltanen et al., 2000), which is based on the global uniqueness proof of Nachman (Nachman, 1995). Both approaches are noniterative and take the full nonlinearity of the EIT reconstruction problem into account.

The layer-stripping algorithm is based on the idea of first finding the conductivity near the boundary of the body using boundary data. Then, using a differential equation of the Ricatti type, boundary data in an interior surface are synthesized, which allows the conductivity estimation in this interior layer. Finally, by repeating the process and stripping layer

[10] Strictly speaking, this technique leads to an asymptotic solution and the approximation amounts to using only the first term of the asymptotic expansion.

by layer, the entire medium is covered. It is a fast method, but it has not yet been shown to perform well with noisy data.

The proof of the global uniqueness by Nachman (1995) is also constructive. In particular, it reduces the nonlinear EIT reconstruction problem to the problem of solving two linear integral equations. This reconstruction algorithm uses the Dirichlet-to-Neumann map, and the conductivity distribution is obtained by using an approximate scattering transform (Isaacson et al., 2006; Siltanen et al., 2000). The $\bar{\partial}$ method has yielded some encouraging results (Isaacson et al., 2006). However, it is only a 2D method at the moment and is better suited to industrial applications.

3. RESEARCH ISSUES AND KEY PROBLEM AREAS OF EIT

3.1. Three-Dimensionality

To date, most published work on EIT image reconstruction has concentrated on solving the 2D problem. The main reasons for this have been speed, cost, and electrode attachment. However, real objects of interest (for example, human patients) are 3D. Most importantly, the information that planar EIT voltage measurements contain is inadequate or even misleading about recovering the conductivity distribution in the same plane because a change of conductivity in any voxel of the imaging object affects all voltage measurements. This feature is distinctive for EIT and results in this technique being characterized as ''soft-field'' tomography as opposed to the ''hard-field'' tomographic techniques (such as X-ray CT) where the attenuation effect on a beam of X-rays depends only on the absorption coefficient of the tissue through which the beam passes, and therefore only that part of the region that intersects the projection path affects the measurement. A physical explanation for the above distinction also can be obtained by the fact that in X-ray CT, the beams of X-rays pass through the body with no significant divergence or deviation, whereas in EIT the injected currents cannot be confined to flow in a plane through a 3D object but spread out in three dimensions.

As a consequence, it is incorrect to obtain a 3D conductivity distribution by superimposing a set of independently recovered 2D images. Therefore, it is necessary to reconstruct a full 3D image from data collected over the entire surface of the object. A major problem in 3D imaging is the necessity to place perhaps a few hundred electrodes over the entire surface of the object. Such electrode attachment problems are usually solved by applying belts or vests of electrodes. Another problem related to 3D imaging is that it is computationally demanding. As a matter of fact, 3D reconstruction in EIT seemed quite formidable until recently, principally because of the need to solve the forward problem in three dimensions. Only during the past few years have computers begun to approach the speed and memory needed. The use of EIT to produce 3D images that are clinically useful is still in its infancy, and the successes that have been reported by Blue et al. (2000), Metherall et al. (1996), Molinari et al. (2001b), Tidswell et al. (2001b), and Vauhkonen et al. (1999) deal mainly with the linearized inverse problem. Regardless of these problems, 3D imaging for EIT is a goal worthy of pursuit.

3.2. Ill-posedness, Sensitivity Considerations and Possible Sources of Error

The main factor that limits the quality of reconstructed conductivity images is the ill-posed nature of the inverse EIT problem. The root of the ill-posedness lies in the combination of the following two facts: (1) EIT is a ''soft-field'' technique—any measurement is affected by the conductivity anywhere in the domain, and (2) for the conductivity reconstruction, one is limited to a set of surface measurements that are far from the most internal parts of the volume being imaged.

The discrete version of Eq. (1) allows us to express any measurement potential as the weighted average of the neighboring potentials, where the weights are nonlinear functions of conductivity values of the related voxels. By repeating this process for all measurements—again and again—while heading toward the center of the object, the voltage measurements are entangled in the global conductivity distribution, and it is easy to see that any internal conductivity value has little influence on the boundary measurements because it is some distance from the measurement points. This causes EIT to have inherently less sensitivity in central conductivity elements and the greatest sensitivity for peripheral conductivity elements. Following the same line of reasoning, small errors in the measurements can be translated into arbitrarily large errors in the computed conductivity distribution, especially toward the central areas of the object.

To increase EIT's ability to discern conductivity changes that occur toward the center of the object, we can apply additional internal electrodes, for example, subdural electrodes during brain surgery (Boone et al., 1994) or reference electrode in the esophagus (Schuessler & Bates, 1995). In this way, the sensitivity in the central region is increased as more data are collected and current reaches more locations compared with surface electrodes only. Moreover, different applied current patterns have different sensitivities (Bayford et al., 1996; Cheney et al., 1999; Vauhkonen et al., 1999; Wang et al., 1992; Yorkey, 1990), and it has been shown by Gisser et al. (1987) that for any initial conductivity distribution there exists a ''best'' current pattern for maximizing sensitivity. Attempts to determine

Comp. by: pg1384Alex, Monica Stage: Proof ChapterID: 0001157249AIEP978-0-12-381316-9 Date:22/4/10 Time:12:24:31
File Path:\\pchns1002z\WOMAT\Production\PRODENV\0000000001\0000018453\0000000016\0001157249.3d
Acronym:AIEP Volume:16204

and apply such patterns are referred to as adaptive techniques (Gisser et al., 1988, 1990; Isaacson & Cheney, 1996; Newell et al., 1988; Paulson et al., 1993; Simske, 1987). In addition, Gisser et al. (1990) have shown that as the number of electrodes increases, the application of a current between a pair of them only, results in worse sensitivity. This suggests that to improve sensitivity when increasing the number of electrodes, we should apply distributed current patterns.

Due to the high sensitivity to voltage measurement errors previously described, greater attention should be paid to the elimination of any error on the voltage measurements, and extensive research has been expended on achieving accurate voltage measurement collection. Next, we discuss the most common sources of error in voltage measurements in EIT.

One possible cause of error on the voltage measurements is the thermal noise, or the intrinsically low signal-to-noise ratio (SNR). Voltages at the measuring electrodes may be as low as a few tens of microvolts. The magnitude of the measured voltage also depends on the magnitude of the current applied. When imaging small physiological changes, the change in electrode voltage might be less than 1%. Thus, voltage changes to be measured may be as little as 0.1 μV. This is approximately equivalent to the thermal noise obtained by measuring the voltage across a 1-KΩ resistor with a bandwidth of 1 KHz. Thermal noise, which is ubiquitous, is a limiting factor in EIT measurement accuracy. In practice, the noise level can be reduced by averaging a set of measurements at the expense of a reduction in acquisition speed. We can also increase the SNR by using parallel data collection systems with as many differential amplifiers as there are electrode pairs. Such systems yield lower noise levels than serial data collection systems. In addition, it has been argued by Isaacson (1986) that a significant improvement in the SNR can be obtained by using optimal distributed current injection patterns, compared with the simpler two-electrode current pattern. Of note, as the number of electrodes increases, the use of optimal current patterns becomes more significant. However, the optimal current densities cannot be known in advance because they depend on the unknown conductivity inside the body. So, the additional computation and hardware required are considerable and may outweigh the improved SNR.

Another principal source of error in the voltage measurements is electrode impedance. If we measure voltage on electrodes through which current is simultaneously flowing, then the voltage measured is not actually that on the body surface, because of the presence of an electrode impedance, generally unknown, between the electrode and the body surface. Electrode impedance is generally not considered a problem in obtaining voltage measurements on electrodes through which current is not flowing, provided a voltmeter with sufficiently high input impedance is used. Even if we use the same electrode at different times in the data collection cycle for driving current and making voltage measurements, the possibility of leakage currents exists. Separate electrodes should also be used for voltage measurements and current injections even in systems with distributed current patterns. Electrode impedance is high at low frequencies—making it difficult to inject currents—and falls with frequency. Hence, the significance of electrode contact impedance can be reduced by obtaining the measurements at the highest possible frequency. One method to eliminate the effect of electrode impedance is to use magnetic inductive tomography (Scharfetter et al., 2005), which does not require electrical contact with the human body.

Parasitic capacitances associated with the input leads and circuitry also can introduce large errors and phase shifts into the voltage measurements, especially at high frequencies. To reduce the corrupting influence of stray capacitances on the measurements, we use a differential amplifier and common mode feedback. In this way, we also overcome the limited high-frequency common mode rejection ratio of operational amplifiers. However, common mode feedback requires (Seagar & Brown, 1987) the use of serial collection of the voltage measurements, which in turn results in lower SNR, which, to some extent, defeats the purpose of using common mode feedback.

Errors in the voltage measurements can also occur because of the quantization process. The measurements obtained for EIT are eventually processed by a computer to reconstruct the image. We can achieve sufficiently low quantization noise by using an analog-to-digital converter (ADC) with a sufficient number of bits. A small dynamic range for the voltage measurements would also be advantageous to minimize quantization noise. To achieve a small dynamic range, we must use as many electrodes as possible and adopt an appropriate measurement strategy (Seagar & Brown, 1987).

3.3. Spatial Resolution Considerations

Spatial resolution imposes a serious constraint on clinical applications of EIT. As described in Section 2.2, the number of independent voltage measurements is limited, which results in a limited number of pixels into which conductivity values can be placed. If we desire to achieve higher spatial resolution, we should increase the number of electrodes so that the number of independent voltage measurements also increases.

However, by doing so, various practical problems arise. First, the practical problem of attaching the electrodes to the patient becomes more significant. Pregelled Ag/AgCl electrodes can be used to deal this problem. Also, electrode belts and vests have been proposed (McAdams et al., 1994). Moreover, the difficulty in maintaining an adequate SNR increases (Seagar & Brown, 1987). Indeed, as the number of electrodes increases, the spacing between them is reduced, leading to even smaller values for the voltage measurements, and the SNR is degraded (Seagar & Brown, 1987) due to the multiplexing operation that occurs in the collection of the voltage measurements. The reduced spacing between the electrodes as their number increases also results in increasing voltage offsets and phase shifts in the measurements, due to current paths through stray capacitances and electrode impedance. In addition, by increasing the number of electrodes for better spatial resolution, the ill-posed nature of the inverse EIT problem becomes more pronounced, as discussed in. 3.2. The reduction in quality caused by these factors may overtake the benefit of the additional information gained by adding electrodes.

3.4. Anisotropy

The reconstruction approaches discussed in this chapter make the tacit assumption that the conductivity distribution to be recovered is isotropic. However, this assumption is not valid for some human tissues—for example, muscle tissue. Although unique solutions for conductivity are possible for isotropic conductors, Kohn & Vogelius (1984a,b) and Sylvester & Uhlmann (1986) have shown that for anisotropic conductors unique solutions for conductivity do not exist. There are several sets of different anisotropic conductivity distributions that give rise to the same surface voltage distribution and which, therefore, cannot be distinguished by these measurements.

The degree to which anisotropy inhibits useful image reconstruction is still an active research topic. Methods that use tensor theory and combine EIT with MRI have been proposed (Seo et al., 2004) as a solution to the problem of recovering an anisotropic conductivity distribution. In addition, data from diffusion tensor MRI have been used (Abascal et al., 2008) to incorporate information about brain tissue anisotropy into the FEM model, when solving the forward EIT problem.

3.5. Difference Imaging

Ideally, the aim of EIT is to reconstruct images of the absolute distribution of conductivity, also known as static images. However, this can be difficult because a high degree of accuracy cannot be achieved in the solution of the forward problem, where precise computer models of the body and the electrodes are required. In difference (dynamic) imaging, we image changes of conductivity with time, rather than absolute values, by assuming that changes in surface voltage measurements are mainly due to conductivity changes, since the electrode configuration and body shape remain almost the same. This results in less illconditioning. Furthermore,

Comp. by: pg1384Alex, Monica Stage: Proof ChapterID: 0001157249AIEP978-0-12-381316-9 Date:22/4/10 Time:12:24:31
File Path:\\pchns1002z\WOMAT\Production\PRODENV\0000000001\0000018453\0000000016\0001157249.3d
Acronym:AIEP Volume:16204

the effects of body shape and electrode configuration, two of the largest sources of error, cancel out. Due to its simplicity, this algorithm has found widespread use in a variety of clinical applications.

3.6. Multifrequency Measurements

As an alternative to changes in time, differential algorithms can image changes in conductivity with frequency (Brown et al., 1994, 1995). In this case, measurements are made over a range of frequencies, and differential images are obtained using data from the lowest frequency (reference frequency) and the other frequencies in turn. This process is also referred to as EIT spectroscopy and allows tissue characterization by using the conductivity spectrum.

Multifrequency measurement is another means of reducing the dependence on body shape and electrode configuration. For this approach to be successful, it is important that there is a large conductivity variation with frequency and that it is different for different tissues. Although images of the absolute conductivity distribution are not produced by EIT spectroscopy, we can obtain images of absolute tissue properties. Hence, multifrequency measurements allow us to obtain anatomical information from dynamic images. A measurement of the ratio of intracellular to extracellular volume can be made in this way, since at low frequencies the current flows around cells and at high frequencies the current can penetrate the cell membrane and flow through intracellular space. Multifrequency EIT systems also have been found to give promising results for the detection of breast malignancies (Glickman et al., 2002; Kerner et al., 2002; Osterman et al., 2000).

4. APPLICATION AREAS OF EIT

There is no doubt that EIT presents many clinical strengths that are related to its distinct features described in the Introduction. For clinical situations in a variety of pathologies it would be desirable to use EIT as a portable means to achieve continuous bedside monitoring of the conductivity distribution inside the body.

Some medical applications of EIT, that have been considered and in which EIT provides advantages over existing techniques are related to the function of the digestive system. These include study of gastric emptying (Avill et al., 1987; Evans & Wright, 1990; Mangnall et al., 1987; Nour, 1992; Sutton & McClelland, 1983), diagnosis of hypertrophic pyloric stenosis (Lamont et al., 1988), diagnosis of diabetes mellitus (Vaisman et al., 1999), detection of gastric motility (Smallwood et al., 1993), detection of abnormalities of the migrating motor complex (Wright & Evans, 1990), effects of stress (Akkermans et al., 1993), management of newborns recovering from intensive care (Devane, 1993), study of gastric acid secretion (Baxter et al., 1988), study of gastric transport (Kotre, 1996; Smallwood et al., 1994), and gastric pH measurement (Watson et al., 1996). Regarding the study of the function of the digestive system, EIT does not require radioactive tracers and gamma cameras as gamma scintigraphy does and is not as uncomfortable as intubation (Dijkstra et al., 1993).

EIT may also be advantageous in monitoring the function of the respiratory system. Applications that have been considered include lung ventilation monitoring (Frerichs et al., 1999a; Khambete et al., 2000; Kunst et al., 1998; Mueller et al., 2001), pulmonary perfusion study (Kunst et al., 1998; McArdle et al., 1988; Mueller et al., 2001), detection of pulmonary embolus (Leathard et al., 1994), mapping of changes in pulmonary resistivity during inspiration with application in the detection of emphysematous bullae (Harris et al., 1987), imaging of pulmonary edema (i.e., increased volume of fluid in the lungs) (Newell et al., 1996), assessment of lung water in neonates and adults with heart failure (Noble et al., 1999), optimization of ventilation during anesthesia and for artificially ventilated patients (Frerichs, 2000; Frerichs et al., 1999b) and lung composition (Brown et al., 1994, 1995; Nopp et al., 1997). Compared with other conventional techniques for monitoring the pulmonary function (e.g, scintigraphy and respiratory inductance plethysmography), EIT offers more spatial information, is less invasive, and does not require difficult calibration (Dijkstra et al., 1993).

In addition to the preceding medical uses, EIT may benefit monitoring of the cardiovascular system. Related applications involve measurement of cardiac output (Eyuboglu et al., 1987, 1989; Hoetink et al., 2002; McArdle et al., 1993; Patterson et al., 2001), detection of deep venous thrombosis (Kim et al., 1989), blood flow imaging (Brown et al., 1991), and diagnosis of pelvic congestion (Thomas et al., 1991).

EIT has great potential in the area of brain imaging. Possible applications are imaging of neural activity (FreygangJr & Landau, 1955; Holder et al., 1996; Tidswell et al., 2001a,b; Van Harreveld & Ochs, 1956), detection of the onset of intraventricular hemorrhage in premature (and of low-birth-weight) infants (Ellison & Evers, 1981; Murphy et al., 1987; Reigel et al., 1977; Tarassenko et al., 1983, 1985; Tarassenko & Rolfe, 1984), imaging of cortical spreading depression (Boone et al., 1994), assessment of the severity of stroke (Holder, 1992), detection of epileptic activity (Bagshaw et al., 2001; Fabrizi et al., 2006; Lux et al., 1986), and development of more accurate models in forward electroencephalography (Gonçalves & de Munck, 2000; Gonçalves et al., 2000, 2003). In detecting the occurrence of seizures, continuous monitoring is necessary; hence, EIT is better suited than functional MRI (Bayford, 2006). However, the main difficulty in using EIT to monitor human brain conductivity is the presence of the highly resistive skull. At the frequencies used by EIT systems, the conductivity of the skull is approximately 30 times less than that of the surrounding scalp (Geddes & Baker, 1967). This effectively shunts most of the current through the scalp. Hence, the amount of current that can flow through the brain is restricted, and the temporal variations in the potential differences to be recorded by the EIT system are relatively small. In addition, the reconstruction problem becomes more ill-posed. To deal with this problem to some degree, diametric current injection, rather than the usual adjacent injection strategy, and time-averaging of many individual measurements have been applied (Bayford et al., 1996).

The early detection of cancerous breast tumors increases the chances of survival dramatically. Hence, EIT also may be of value in breast cancer screening by imaging breast tissue (Cherepenin et al., 2002; Jossinet & Schmitt, 1999; Korjenevsky et al., 2001; Trokhanova et al., 2001; Ultchin et al., 2002). Promising results for the detection of breast malignancies have also been obtained from multifrequency EIT systems (Glickman et al., 2002; Kerner et al., 2002; Osterman et al., 2000). EIT performs better than X-ray mammography because it results in lower false-positive and false-negative rates, especially in women whose breast tissue is dense (Bayford, 2006). EIT also may be used to control irradiation doses for cancer treatment (Osterman et al., 1999).

The reduction of tumor size may be achieved by using hyperthermia treatment. To control hyperthermia treatment, a method is required to calculate the thermal distribution of the heated tissue. Since there is a linear dependency between tissue temperature and tissue resistivity (Bayford, 2006), it has been suggested by Amasha et al. (1988), Conway (1987), Conway et al. (1992, 1985), Griffiths & Ahmed (1987), and Möller et al. (1993) that EIT be used for this purpose. EIT has been found more accurate than other invasive methods that use thermocouples or thermistors (Dijkstra et al., 1993).

EIT may be of value to the function of the myoskeletal system. Since bone fractures lead to formation of hematomas at the fracture site, it is expected that EIT may be used to identify the fracture site and to monitor the stages of fracture healing. Preliminary studies have been considered (Ritchie et al., 1989) and in contrast to other radiographic methods, EIT can assess early changes of fracture healing.

Other health-related applications of EIT include esophageal activity measurement with a view to detect swallowing disorders (e.g., Parkinson's disease (Erol et al., 1996; Hughes et al., 1994)), measurement of lean/fat ratios (investigation of nutrition) (Brown et al., 1988), measurement of changes following exercise (Elleby et al., 1990), tissue characterization (Brown et al., 2000), determination of the boundary between dead and living tissue (Cheney et al., 1999), and determination of the intracellular-to-extracellular volume ratio (Brown, 2001).

Although most current interest is in the use of EIT for medical imaging, there is also some interest in its use in geophysical and industrial measurements. Geophysical applications include detection of buried objects or buried historic buildings (Szymanski & Tsourlos, 1993), determination of differing geological formations, determination of the location of mineral deposits in the Earth (Dines & Lytle, 1981; Parker, 1984; Stefanesco et al., 1930), tracing of the spreads of contaminants in the Earth (Daily & Ramirez, 1995; Ramirez et al., 1993, 1996), and core sample analysis, where a cylindrical section of Earth is placed in a pressure vessel and the effects of various pressure and temperature conditions are visualized. In addition, EIT could be applied usefully in industrial testing—for instance, to determine the existence and length of internal cracks in materials (Alessandrini & Rondi, 1998; Friedman & Vogelius, 1989; Kaup et al., 1996). Other industrial applications are the nondestructive evaluation of machinery parts (Eggleston et al., 1990) and the control of industrial processes such as curing and cooking. Nonmedical applications of EIT also lie in process tomography, where we want to obtain images of either the distribution of the contents of a pipeline or the multiphase flow of substances in a mixing vessel (Dyakowski, 1996; Jaworski & Dyakowski, 2001; Williams & Beck, 1995; Xie et al., 1991; Yang et al., 1995). Finally, situations exist in which imaging of fluidization processes is desirable (Liu et al., 2002).

5. CONCLUSIONS AND FUTURE RESEARCH

EIT has slowly established itself as a routine clinical tool. The factors limiting the quality of the reconstructed images have been discussed. These factors make it unlikely that EIT images will ever achieve resolution comparable with that of anatomical images obtained by X-ray CT and MRI. However, EIT might compete as a functional imaging modality with other modalities of this type—for example, functional MRI. The fact that useful images have been obtained suggests that the related problems of EIT are not insurmountable.

It is likely that future EIT systems will be smaller and have wider bandwidth. They may be completely wireless and use the latest developments of wireless local area networks to return data to microprocessors. Another subject likely to be heavily researched over the next few years is absolute conductivity imaging in three dimensions. In general, future research should address all the deficiencies of the current EIT reconstruction algorithms as mentioned in Section 2. It is still unknown whether the development and use of nano-electrodes will result in a net improvement in EIT image quality as a result of the increased number of electrodes.

Comp. by: pg1384Alex, Monica Stage: Proof ChapterID: 0001157249AIEP978-0-12-381316-9 Date:22/4/10 Time:12:24:32
File Path:\\pchns1002z\WOMAT\Production\PRODENV\0000000001\0000018453\0000000016\0001157249.3d
Acronym:AIEP Volume:16204

Much research is dedicated to combine EIT, with its excellent temporal resolution, with other modalities of better spatial resolution. In this direction, an interesting development is magnetic resonance electrical impedance tomography (Gao et al., 2005), a new imaging technique that integrates EIT into an MRI system. In this technique, a low-frequency current is injected through a pair of boundary electrodes and the distribution of the induced magnetic flux density within the body is measured by an MRI scanner. Subsequently, the current density distribution inside the body is obtained by using Ampere's law. Finally, the conductivity distribution of the body is estimated using the relationship between conductivity and current density.

6. APPENDICES

A. *Differential Operators of Space*

DEFINITIONS

1. Gradient of a scalar function $f(x,y,z)$ in Cartesian coordinates:

$$\operatorname{grad} f = \nabla f = \frac{\partial f(x,y,z)}{\partial x}\hat{\mathbf{x}} + \frac{\partial f(x,y,z)}{\partial y}\hat{\mathbf{y}} + \frac{\partial f(x,y,z)}{\partial z}\hat{\mathbf{z}}. \tag{A-1}$$

2. Divergence of a vector field $\bar{\mathbf{v}}(x,y,z) = v_x\hat{\mathbf{x}} + v_y\hat{\mathbf{y}} + v_z\hat{\mathbf{z}}$ in Cartesian coordinates:

$$\operatorname{div}\bar{\mathbf{v}} = \nabla\cdot\bar{\mathbf{v}} = \frac{\partial v_x}{\partial x} + \frac{\partial v_y}{\partial y} + \frac{\partial v_z}{\partial z}. \tag{A-2}$$

3. Rotation of a vector field $\bar{\mathbf{v}}(x,y,z) = v_x\hat{\mathbf{x}} + v_y\hat{\mathbf{y}} + v_z\hat{\mathbf{z}}$ in Cartesian coordinates:

$$\begin{aligned}\operatorname{rot}\bar{\mathbf{v}} = \operatorname{curl}\bar{\mathbf{v}} = \nabla\times\bar{\mathbf{v}} &= \begin{vmatrix} \hat{\mathbf{x}} & \hat{\mathbf{y}} & \hat{\mathbf{z}} \\ \dfrac{\partial}{\partial x} & \dfrac{\partial}{\partial y} & \dfrac{\partial}{\partial z} \\ v_x & v_y & v_z \end{vmatrix} \\ &= \left(\frac{\partial v_z}{\partial y} - \frac{\partial v_y}{\partial z}\right)\hat{\mathbf{x}} + \left(\frac{\partial v_x}{\partial z} - \frac{\partial v_z}{\partial x}\right)\hat{\mathbf{y}} + \left(\frac{\partial v_y}{\partial x} - \frac{\partial v_x}{\partial y}\right)\hat{\mathbf{z}}.\end{aligned} \tag{A-3}$$

4. Laplacian operator of a scalar function $f(x, y, z)$ in Cartesian coordinates:

$$\nabla f(x,y,z) = \nabla f \cdot \nabla f = \nabla^2 f = \frac{\partial^2 f}{\partial x^2} + \frac{\partial^2 f}{\partial y^2} + \frac{\partial^2 f}{\partial z^2}. \tag{A-4}$$

RULES OF CALCULATION

1. If f is a scalar function and $\bar{\mathbf{v}}$ is a vector field, then

$$\operatorname{div} f\bar{\mathbf{v}} = \nabla \cdot f\bar{\mathbf{v}} = \bar{\mathbf{v}} \cdot \nabla f + f\nabla \cdot \bar{\mathbf{v}}. \tag{A-5}$$

2. If c is a constant, then

$$\operatorname{grad} c = \nabla c = \overline{0}. \tag{A-6}$$

3. If f is a scalar function and $\bar{\mathbf{v}}$ is an arbitrary vector, then the directional derivative $\nabla_{\bar{\mathbf{v}}} f$ is the rate at which function f changes in the direction of vector $\bar{\mathbf{v}}$:

$$\nabla_{\bar{\mathbf{v}}} f = \nabla f \cdot \frac{\bar{\mathbf{v}}}{|\bar{\mathbf{v}}|}. \tag{A-7}$$

If the directional vector is the outward normal unit $\hat{\mathbf{n}}$ on a boundary $\partial\Omega$, then the directional derivative is called the normal derivative of f to $\partial\Omega$. It is denoted by $\frac{\partial f}{\partial n}$ and is given by the following dot product:

$$\frac{\partial f}{\partial n} = \nabla f \cdot \hat{\mathbf{n}}. \tag{A-8}$$

4.

$$\nabla F(U) = F'(U)\nabla U. \tag{A-9}$$

B. Derivation of Eqs. (1) and (2) from Maxwell's Equations

In general, the electromagnetic field in a medium is described by the system of Maxwell's equations. However, due to the frequency range at which EIT systems operate and the size of objects to which it is applied, the electric and magnetic fields are decoupled. Hence, we can use the following quasi-static approximation of Maxwell's equations:

$$\nabla \times \boldsymbol{E} = 0 \tag{B-1}$$

$$\nabla \cdot \boldsymbol{J} = 0, \tag{B-2}$$

where $\boldsymbol{E}$ denotes the electric field density observed in a volume Ω bounded by a surface $\partial\Omega$ and $\boldsymbol{J}$ is the conduction current density. Eq. (B-2) simply states that the sum of all the currents entering the volume is zero (Kirchoff's second law). Eq. (B-1) enables us to introduce the electric scalar potential u as

$$\boldsymbol{E} = -\nabla u. \tag{B-3}$$

Considering Ohm's law:

$$\boldsymbol{J} = \sigma \boldsymbol{E}, \tag{B-4}$$

where σ is the conductivity profile and also taking into account Eq. (B-3), Eq. (B-2) yields the following partial differential equation (Poisson's equation) for u:

$$\nabla \cdot (\sigma \nabla u) = 0. \tag{B-5}$$

For EIT, the normal component (with respect to $\partial\Omega$) of the total current density $\boldsymbol{J}$ should be equal to the applied current density ψ

$$\boldsymbol{J} \cdot (-\boldsymbol{n}) = \psi, \tag{B-6}$$

where $\boldsymbol{n}$ is the outward normal unit on $\partial\Omega$. This equation, when combined with Eq. (B-3) and Eq. (B-4), leads to the Neuman boundary condition

$$\sigma \frac{\partial u}{\partial n} = \psi, \tag{B-7}$$

where $\frac{\partial u}{\partial n}$ denotes the normal derivative of u to $\partial\Omega$ (i.e., the rate at which the scalar electric potential u changes in the direction of $\boldsymbol{n}$), given by the dot product:

$$\frac{\partial u}{\partial n} = \nabla u \cdot \boldsymbol{n}. \tag{B-8}$$

ACKNOWLEDGMENTS

This work was supported by the Engineering and Physical Sciences Research Council (EPSRC) portfolio ''Integrated Electronics.''

REFERENCES

Abascal, J. F. P. J., Arridge, S. R., Atkinson, D., Horesh, R., Fabrizi, L., De Lucia, M., et al. (2008). Use of anisotropic modelling in electrical impedance tomography; description of method and preliminary assessment of utility in imaging brain function in the adult human head. *NeuroImage*, *43*(2), 258–268.

Akkermans, L. M. A., Tekamp, F. A., Smout, A. J. P. M., Roelofs, J. M. M., & Wiegant, V. M. (1993). The effects of stress on gastric emptying as measured by electrical impedance tomography (EIT). In D. S. Holder (Ed.), *Clinical and Physiological Applications of Electrical Impedance Tomography* (pp. 107–112). London: UCL Press.

Alessandrini, G., & Rondi, L. (1998). Stable determination of a crack in a planar inhomogeneous conductor. *SIAM J. Math. Anal.*, *30*(2), 326–340. Au2

Allers, A., & Santosa, F. (1991). Stability and resolution analysis of a linearized problem in electrical impedance tomography. *Inverse Problems*, *7*(4), 515–533.

Amasha, H. M., Anderson, A. P., Conway, J., & Barber, D. C. (1988). Quantitative assessment of impedance tomography for temperature measurements in microwave hyperthermia. *Clinical Physics and Physiological Measurement*, *9*(Suppl. A), 49–53.

Avill, R., Mangnall, Y. F., Bird, N. C., Brown, B. H., Barber, D. C., Seagar, A. D., et al. (1987). Applied potential tomography: a new non invasive technique for measuring gastric emptying. *Gastroenterology*, *92*, 1019–1026.

Babaeizadeh, S., Brooks, D. H., & Isaacson, D. (2004). A 3-D boundary element solution to the forward problem of electrical impedance tomography. In *Proc. 26th Annu. Int. Conf. IEEE Eng. Med. Biol. Soc. (EMBS)* (pp. 960–963). September 1–5 San Francisco, CA, USA. Au2

Bagshaw, A. P., Eadie, L. H., Binnie, C., Tidswell, R. J., Yerworth, R. J., Bayford, R. H., et al. (2001). Imaging of interictal epileptiform activity using electrical impedance tomography. In *Proc. XIth Int. Conf. on Electrical Bio-impedance (ICEBI)* (pp. 473–477). June 17–21 Oslo, Norway. Au2

Bagshaw, A. P., Liston, A. D., Bayford, R. H., Tizzard, A., Gibson, A. P., Tidswell, A. T., et al. (2003). Electrical impedance tomography of human brain function using reconstruction algorithms based on the finite element method. *NeuroImage*, *20*(2), 752–764.

Barber, D. C. (1995). Electrical impedance tomography. In J. D. Bronzino (Ed.), *The Biomedical Engineering Handbook* (pp. 1151–1164). Boca Raton, FL, USA: CRC Press.

Barber, D. C., & Brown, B. H. (1984). Applied potential tomography. *Journal of Physics E: Scientific Instruments*, *17*(9), 723–733.

Barber, D. C., & Brown, B. H. (1985). Recent developments in applied potential tomography. In *Proc. 9th Conf. on Inf. Process. Med. Imaging (IPMI)* (pp. 106–121). June 10–14 Washington, DC, USA. Au2

Baxter, A. J., Mangnall, Y. F., Loj, E. H., Brown, B., Barber, D. C., Johnson, A. G., et al. (1988). Evaluation of applied potential tomography as a new non-invasive gastric secretion test. *Gut*, *29*(12), 1730–1735.

Bayford, R. H. (2006). Bioimpedance tomography (electrical impedance tomography). *Annual Review of Biomedical Engineering*, *8*, 63–91.

Bayford, R. H., Boone, K. G., Hanquan, Y., & Holder, D. S. (1996). Improvement of the positional accuracy of EIT images of the head using a Lagrange multiplier reconstruction algorithm with diametric excitation. *Physiological Measurement*, *17*(Suppl. 4A), A49–A57.

Bayford, R. H., Gibson, A., Tizzard, A., Tidswell, T., & Holder, D. S. (2001). Solving the forward problem in electrical impedance tomography for the human head using IDEAS (integrated design engineering analysis software), a finite element modelling tool. *Physiological Measurement*, *22*(1), 55–64.

Beylkin, G. (1984). The inversion problem and applications of the generalized Radon transform. *Commun. Pure Appl. Math.*, *37*(5), 579–599. Au2

Beylkin, G. (1985). Imaging of discontinuities in the inverse scattering problem by inversion of a causal generalized Radon transform. *J. Math. Phys.*, *26*(1), 99–108. Au2

Blott, B. H., Cox, S. J., Daniell, G. J., Caton, M. J., & Nicole, D. A. (2000). High fidelity imaging and high performance computing in nonlinear EIT. *Physiological Measurement*, *21*(1), 7–14.

Blue, R. S., Isaacson, D., & Newell, J. C. (2000). Real-time three-dimensional electrical impedance imaging. *Physiological Measurement*, *21*(1), 15–26.

Boone, K., Barber, D., & Brown, B. (1997). Imaging with electricity: report of the European Concerted Action on Impedance Tomography. *Journal of Medical Engineering and Technology*, *21*(6), 201–232.

Boone, K., Lewis, A. M., & Holder, D. S. (1994). Imaging of cortical spreading depression using EIT: implications for localization of epileptic foci. *Physiological Measurement*, *15*(Suppl. 2A), A189–A198.

Borsic, A., Lionheart, W. R. B., & McLeod, C. N. (2002). Generation of anisotropic-smoothness regularization filters for EIT. *IEEE Transactions on Medical Imaging*, *21*(6), 579–587.

Brenner, S. C., & Scott, L. R. (1994). *The Mathematical Theory of Finite Element Methods*. New York: Springer-Verlag.

Brown, B. H. (2001). Medical impedance tomography and process impedance tomography: a brief review. *Measurement Science & Technology*, *12*(8), 991–996.

Brown, B. H. (2003). Electrical impedance tomography (EIT): a review. *Journal of Medical Engineering and Technology*, *27*(3), 97–108.

Brown, B. H., Barber, D. C., Wang, W., Lu, L., Leathard, A. D., Smallwood, R. H., et al. (1994). Multi-frequency imaging and modelling of respiratory related electrical impedance changes. *Physiological Measurement*, *15*(Suppl. 2A), A1–A12.

Brown, B. H., Karatzas, T., Nakienly, R., & Klarke, R. G. (1988). Determination of upper arm muscle and fat areas using electrical impedance measurements. *Clinical Physics and Physiological Measurement*, *9*(1), 47–55.

Brown, B. H., Leathard, A., Sinton, A., McArdle, F. J., Smith, R. W. M., & Barber, D. C. (1991). Blood flow imaging using electrical impedance tomography. In *Proc. 13th Annu. Int. Conf. IEEE Eng. Med. Biol. Soc. (EMBS)* (pp. 307–308). October 31–November 3, Orlando, FL, USA. Au2

Brown, B. H., Leathard, A. D., Lu, L., Wang, W., & Hampshire, A. (1995). Measured and expected Cole parameters from electrical impedance tomographic spectroscopy images of the human thorax. *Physiological Measurement*, *16*(Suppl. 3A), A57–A67.

Brown, B. H., Tidy, J. A., Boston, K., Blackett, A. D., Smallwood, R. H., & Sharp, F. (2000). Relation between tissue structure and imposed electrical current flow in cervical neoplasia. *Lancet*, *355*(9207), 892–895.

Burnett, D. S. (1987). *Finite Element Analysis: From Concepts to Applications*. Reading, MA, USA: Addison-Wesley.

Calderón, A. P. (1980). On an inverse boundary value problem. In *Seminar on Numerical Analysis and Its Applications to Continuum Physics* (pp. 65–73). Rio de Janeiro: Soc. Brasileira de Matemática.

Cheney, M., Isaacson, D., & Isaacson, E. L. (1990). Exact solutions to a linearized inverse boundary problem. *Inverse Problems*, *6*(6), 923–934. Au1

Cheney, M., Isaacson, D., & Newell, J. C. (1999). Electrical impedance tomography. *SIAM Rev.*, *41*(1), 85–101. Au2

Cheney, M., Isaacson, D., Newell, J. C., Simske, S., & Goble, J. (1990). NOSER: an algorithm for solving the inverse conductivity problem. *Int. J. Imaging Syst. Technol.*, *2*(2), 66–75. Au1, 2

Cheng, K. S., Isaacson, D., Newell, J. C., & Gisser, D. G. (1989). Electrode models for electric current computed tomography. *IEEE Transactions on Biomedical Engineering*, *36*(9), 918–924.

Cherepenin, V. A., Karpov, A. Y., Korjenevsky, A. V., Kornienko, V. N., Kultiasov, Y. S., Ochapkin, M. B., et al. (2002). Three-dimensional EIT imaging of breast tissues: system design and clinical testing. *IEEE Transactions on Medical Imaging*, *21*(6), 662–667.

Cinel, I., Jean, S., & Dellinger, R. P. (2007). Dynamic lung imaging techniques in mechanically ventilated patients. In J. L. Vincent (Ed.), *Intensive Care Medicine: 2007 Annual Update* (pp. 371–380). Berlin Heidelberg: Springer.

Clay, M. T., & Ferree, T. C. (2002). Weighted regularization in electrical impedance tomography with applications to acute cerebral stroke. *IEEE Transactions on Medical Imaging*, *21*(6), 629–637.

Cohen-Bacrie, C., Goussard, Y., & Guardo, R. (1997). Regularized reconstruction in electrical impedance tomography using a variance uniformization constraint. *IEEE Transactions on Medical Imaging*, *16*(5), 562–571.

Connolly, T. J., & Wall, D. J. N. (1988). On an inverse problem, with boundary measurements, for the steady state diffusion equation. *Inverse Problems*, *4*(4), 995–1012.

Conway, J. (1987). Electrical impedance tomography for thermal monitoring of hyperthermia treatment: an assessment using in vitro and in vivo measurements. *Clinical Physics and Physiological Measurement*, *8*(Suppl. A), 141–146.

Conway, J., Hawley, M., Mangnall, Y., Amasha, H., & van Rhoon, G. C. (1992). Experimental assessment of electrical impedance imaging for hyperthermia monitoring. *Clinical Physics and Physiological Measurement*, *13*(Suppl. A), 185–189.

Conway, J., Hawley, M. S., Seagar, A. D., Brown, B. H., & Barber, D. C. (1985). Applied potential tomography (APT) for noninvasive thermal imaging during hyperthermia treatment. *Electronics Letters*, *21*(19), 836–838.

Courant, R., & Hilbert, D. (1968). *Methoden der Mathematischen Physik*. Berlin: Springer.

Daily, W., & Ramirez, A. (1995). Electrical resistance tomography during in-citu tricholoethylene remediation at the Savannah River Site. *J. Appl. Geophys.*, *33*(4), 239–249.

Devane, S. P. (1993). Application of EIT to gastric emptying in infants: validation against residual volume method. In D. S. Holder (Ed.), *Clinical and Physiological Applications of Electrical Impedance Tomography* (pp. 113–123). London: UCL Press. Au2

Dijkstra, A. M., Brown, B. H., Leathard, A. D., Harris, N. D., Barber, D. C., & Edbrooke, D. L. (1993). Review: clinical applications of electrical impedance tomography. *Journal of Medical Engineering and Technology*, *17*(3), 89–98.

Dines, K. A., & Lytle, R. J. (1981). Analysis of electrical conductivity imaging. *Geophys*, *46*(7), 1025–1036.

Dobson, D. C., & Santosa, F. (1994). An image-enhancement technique for electrical impedance tomography. *Inverse Problems*, *10*(2), 317–334.

Dong, G., Bayford, R. H., Gao, S., Saito, Y., Yerworth, R., Holder, D., & Yan, W. (2003). The application of the generalized vector sample pattern matching method for EIT image reconstruction. *Physiological Measurement*, *24*(2), 449–466.

Dyakowski, T. (1996). Process tomography applied to multi-phase flow measurement. *Measurement Science & Technology*, *7*(3), 343–353.

Eggleston, M. R., Schwabe, R. J., Isaacson, D., & Coffin, L. F. (1990). The application of electric current computed tomography to defect imaging in metals. In D. O. Thompson & D. E. Chimenti (Eds.), *Review of Progress in Quantitative Nondestructive Evaluation* (pp. 455–462). New York: Plenum Press.

Elleby, B., Knudsen, L. F., Brown, B. H., Crofts, C. E., Woods, M. J., & Trowbridge, E. A. (1990). Electrical impedance assessment of muscle changes following exercise. *Clinical Physics and Physiological Measurement*, *11*(2), 159–166.

Ellison, P. H., & Evers, J. (1981). Transcephalic impedance in the neonate: an indicator of intracranial hemorrhage, asphyxia, and delayed maturation. *Journal of Pediatrics*, *98*(6), 968–971.

Erol, R. A., Cherian, P., Smallwood, R. H., Brown, B. H., & Bardhan, K. D. (1996). Can electrical impedance tomomgraphy be used to detect gastro-oesophageal reflux? *Physiological Measurement*, *17*(Suppl. 4A), A141–A147.

Evans, D. F., & Wright, J. W. (1990). Is acid suppression necessary when measuring gastric emptying using applied potential tomography? In T. J. Hames (Ed.), *Proc. of the Copenhagen Meeting on Electrical Impedance Tomography* (pp. 249–255). Sheffield, UK: Sheffield University.

Eyuboglu, B. M., Brown, B. H., & Barber, D. C. (1989). In vivo imaging of cardiac related impedance changes. *IEEE Trans. Med. Biol.*, *8*(1), 39–45. Au2

Eyuboglu, B. M., Brown, B. H., Barber, D. C., & Seagar, A. D. (1987). Localization of cardiac related impedance changes in the thorax. *Clinical Physics and Physiological Measurement*, *8*(Suppl. A), 167–173.

Fabrizi, L., Horesh, L., McEwan, A., & Holder, D. S. (2006). A feasibility study for imaging of epileptic seizures by EIT using a realistic FEM of the head. In *Proc. World Congress Med. Phys. Biomed. Eng.* (pp. 3874–3877). August 27–September 1, Seoul, Korea.

Frerichs, I. (2000). Electrical impedance tomography (EIT) in applications related to lung and ventilation: a review of experimantal and clinical activities. *Physiological Measurement*, *21*(2), R1–R21.

Frerichs, I., Hahn, G., & Hellige, G. (1999). Thoracic electrical impedance tomographic measurements during volume controlled ventilation-effects of tidal volume and positive end-expiratory pressure. *IEEE Transactions on Medical Imaging*, *18*(9), 764–773.

Frerichs, I., Hahn, G., Schiffmann, H., Berger, C., & Hellige, G. (1999). Monitoring regional lung ventilation by functional electrical impedance tomography during assisted ventilation. *Annals of the New York Academy of Sciences*, *873*, 493–505.

FreygangJr, W. H., & Landau, W. M. (1955). Some relations between resistivity and electrical activity in the cerebral cortex of the cat. *Journal of Cellular and Comparative Physiology*, *45*(3), 377–392.

Friedman, A., & Vogelius, M. (1989). Determining cracks by boundary measurements. *Indiana U. Math. J.*, *38*(3), 527–556.

Gao, N., Zhu, S. A., & He, B. (2005). Estimation of electrical conductivity distribution within the human head from magnetic flux density measurement. *Physics in Medicine and Biology*, *50*(11), 2675–2687.

Geddes, L. A., & Baker, L. E. (1967). The specific resistance of biological material—a compendium of data for the biomedical engineering and physiologist. *Medical and Biological Engineering and Computing*, *5*(3), 271–293.

Gersing, E. (1999). Monitoring temperature-induced changes in tissue during hyperthermia by impedance methods. *Annals of the New York Academy of Sciences*, *873*, 13–20.

Geselowitz, D. B. (1971). An application of electrocardiographic lead theory to impedance plethysmography. *IEEE Transactions on Biomedical Engineering*, *18*(1), 38–41.

Gisser, D. G., Isaacson, D., & Newell, J. C. (1987). Current topics in impedance imaging. *Clinical Physics and Physiological Measurement*, *8*(Suppl. 4A), 39–46.

Gisser, D. G., Isaacson, D., & Newell, J. C. (1988). Theory and performance of an adaptive current tomography system. *Clinical Physics and Physiological Measurement*, *9*(Suppl. A), 35–41.

Gisser, D. G., Isaacson, D., & Newell, J. C. (1990). Electric current computed tomography and eigenvalues. *SIAM J. Appl. Math.*, *50*(6), 1623–1634.

Glickman, Y. A., Filo, O., Nachaliel, U., Lenington, S., Amin-Spector, S., & Ginor, R. (2002). Novel EIS postprocessing algorithm for breast cancer diagnosis. *IEEE Transactions on Medical Imaging*, *21*(6), 710–712.

Glidewell, M. E., & Ng, K. T. (1997). Anatomically constrained electrical impedance tomography for three-dimensional anisotropic bodies. *IEEE Transactions on Medical Imaging*, *16*(5), 572–580.

Golub, G. H., & Van Loan, C. F. (1996). *Matrix Computations* (3rd ed.). Baltimore, MD, USA: Johns Hopkins University Press.

Gonçalves, S., & de Munck, J. C. (2000). The use of electrical impedance tomography with the inverse problem of EEG and MEG. In *Proc. 22nd Annu. Int. Conf. IEEE Eng. Med. Biol. Soc. (EMBS)* (pp. 2346–2349). July 23–28, Chicago, IL, USA.

Gonçalves, S., de Munck, J. C., Heethaar, R. M., Lopes da Silva, F. H., & van Dijk, B. W. (2000). The application of electrical impedance tomography to reduce systematic errors in the EEG inverse problem—a simulation study. *Physiological Measurement*, *21*(3), 379–393.

Gonçalves, S. I., de Munck, J. C., Verbunt, J. P. A., Bijma, F., Heethaar, R. M., & Lopes da Silva, F. (2003). In vivo measurement of the brain and skull resistivities using an EIT-based method and realistic models for the head. *IEEE Transactions on Biomedical Engineering*, *50*(6), 754–767.

Grant, F. C. (1923). Localization of brain tumours by determination of the electrical resistance of the growth. *Journal of the American Medical Association*, *81*(26), 2169–2172.

Griffiths, H., & Ahmed, A. (1987). Applied potential tomography for non-invasive temperature mapping in hyperthermia. *Clinical Physics and Physiological Measurement*, *8*(Suppl. A), 147–153.

Hadamard, J. (1923). *Lectures on Cauchy's Problem in Linear Partial Differential Equations*. New Haven, CT, USA: Yale University Press.

Harris, N. D., Suggett, A. J., Barber, D. C., & Brown, B. H. (1987). Applications of applied potential tomography (APT) in respiratory medicine. *Clinical Physics and Physiological Measurement*, *8*(Suppl. A), 155–165.

Helmholtz, H. (1853). Ueber einige Gesetze der Vertheilung elektrischer Ströme in körperlichen Leitern, mit Anwendung auf die thierisch-elektrischen Versuche. *Annalen der Physik und Chemie*, *89*(7), 211–233 353–377.

Hoetink, A. E., Faes, T. J. C., Marcus, J. T., Kerkkamp, H. J. J., & Heethaar, R. M. (2002). Imaging of thoracic blood volume changes during the heart cycle with electrical impedance using a linear spot-electrode array. *IEEE Transactions on Medical Imaging*, *21*(6), 653–661.

Holder, D. S. (1992). Electrical impedance tomography of global cerebral ischaemia with cortical or scalp electrodes in the anaesthetised rat. *Clinical Physics and Physiological Measurement*, *13*(1), 87–98.

Holder, D. S., Rao, A., & Hanquan, Y. (1996). Imaging of physiologically evoked responses by electrical impedance tomography with cortical electrodes in the anaesthetised rabbit. *Physiological Measurement*, *17*(Suppl. 4A), A179–A186.

Hossman, K. A. (1971). Cortical steady potential, impedance and excitability changes during and after total ischemia of cat brain. *Experimental Neurology*, *32*(2), 163–175.

Hsiao, G. C., Schnack, E., & Wendland, W. L. (2000). Hybrid coupled finite-boundary element methods for elliptic systems of second order. *Computer Methods in Applied Mechanics and Engineering*, *190*(5–7), 431–485.

Hua, P., Woo, E. J., & Webster, J. G. (1993). Finite element modeling of electrode-skin contact impedance in electrical impedance tomography. *IEEE Transactions on Biomedical Engineering*, *40*(4), 335–343.

Hua, P., Woo, E. J., Webster, J. G., & Tompkins, W. J. (1991). Iterative reconstruction methods using regularization and optimal current patterns in electrical impedance tomography. *IEEE Transactions on Medical Imaging*, *10*(4), 621–628.

Hughes, T. A. T., Liu, P., Griffiths, H., Lawrie, B. W., & Wiles, C. M. (1994). An analysis of studies comparing electrical impedance tomography with X-ray videofluoroscopy in the assessment of swallowing. *Physiological Measurement*, *15*(Suppl. 2A), A199–A209.

Isaacson, D. (1986). Distinguishability of conductivities by electric current computed tomography. *IEEE Transactions on Medical Imaging*, *5*(2), 91–95.

Isaacson, D., & Cheney, M. (1991). Effects of measurement precision and finite numbers of electrodes on linear impedance imaging algorithms. *SIAM J. Appl. Math.*, *51*(6), 1705–1731.

Isaacson, D., & Cheney, M. (1996). *Process for producing optimal current patterns for electrical impedance tomography*. U. S. Patent, No. 5,588,429, December.

Isaacson, D., & Isaacson, E. L. (1989). Comment on Calderón's paper: on an inverse boundary value problem. *Math. Comput.*, *52*(186), 553–559. Au2

Isaacson, D., Mueller, J. L., Newell, J. C., & Siltanen, S. (2006). Imaging cardiac activity by the D-bar method for electrical impedance tomography. *Physiological Measurement*, *27*(5), S43–S50.

Jain, H., Isaacson, D., Edic, P. M., & Newell, J. C. (1997). Electrical impedance tomography of complex conductivity distributions with non-circular boundary. *IEEE Transactions on Biomedical Engineering*, *44*(11), 1051–1060.

Jaworski, A. J., & Dyakowski, T. (2001). Application of electrical capacitance tomography for measurement of gas-solids flow characteristics in a pneumatic conveying system. *Measurement Science & Technology*, *12*(8), 1109–1119.

Jinchuang, Z., Wenli, F., Taoshen, L., & Shi, W. (2002). An image reconstruction algorithm based on a revised regularization method for electrical capacitance tomography. *Measurement Science & Technology*, *13*(4), 638–640.

Jossinet, J., & Schmitt, M. (1999). A review of parameters for the bioelectrical characterization of breast tissue. *Annals of the New York Academy of Sciences*, *873*, 30–41.

Kaipio, J. P., Kolehmainen, V., Somersalo, E., & Vauhkonen, M. (2000). Statistical inversion and Monte Carlo sampling methods in electrical impedance tomography. *Inverse Problems*, *16*(5), 1487–1522.

Kaipio, J. P., Kolehmainen, V., Vauhkonen, M., & Somersalo, E. (1999). Inverse problems with structural prior information. *Inverse Problems*, *15*(3), 713–729.

Kaup, P. J., Santosa, F., & Vogelius, M. (1996). Method for imaging corrosion damage in thin plates from electrostatic data. *Inverse Problems*, *12*(3), 279–293.

Kerner, T. E., Paulsen, K. D., Hartov, A., Soho, S. K., & Poplack, S. P. (2002). Electrical impedance spectroscopy of the breast: clinical imaging results in 26 subjects. *IEEE Transactions on Medical Imaging*, *21*(6), 638–645.

Khambete, N. D., Brown, B. H., & Smallwood, R. H. (2000). Movement artefact rejection in impedance pneumography using six strategically placed electrodes. *Physiological Measurement*, *21*(1), 79–88.

Kim, Y., Woo, H. W., & Luedtke, A. E. (1989). Impedance tomography and its application in deep venous thrombosis detection. *IEEE Eng. Med. Biol.*, *8*(1), 46–49. Au2

Kleinermann, F., Avis, N. J., Judah, S. K., & Barber, D. C. (1996). Three-dimensional image reconstruction for electrical impedance tomography. *Physiological Measurement*, *17*(Suppl. 4A), A77–A83.

Kohn, R., & Vogelius, M. (1984). Determining conductivity by boundary measurement. *Commun. Pure Appl. Math.*, *37*(3), 289–298. Au2

Kohn, R. V., & Vogelius, M. (1984b). Identification of an unknown conductivity by means of measurements at the boundary. In D. W. McLaughlin (Ed.), *Inverse Problems14*, (pp. 113–123). SIAM-AMS Proc.

Korjenevsky, A. V., Cherepenin, V. A., Karpov, A. Y., Kornienko, V. N., & Kultiasov, Y. S. (2001). An electrical impedance tomography system for 3-D breast tissues imaging. In *Proc. XIth Int. Conf. on Electrical Bio-impedance (ICEBI)* (pp. 403–407). June 17–21, Oslo, Norway.

Kotre, C. J. (1996). Subsurface electrical impedance imaging: measurement strategy, image reconstruction and in vivo results. *Physiological Measurement*, *17*(Suppl. 4A), A197–A204.

Kunst, P. W. A., Vonk Noordegraaf, A., Hoekstra, O. S., Postmus, P. E., & de Vries, P. M. J. M. (1998). Ventilation and perfusion imaging by electrical impedance tomography: a comparison with radionuclide scanning. *Physiological Measurement*, *19*(4), 481–490.

Lamont, G. L., Wright, J. W., Evans, D. F., & Kapila, L. (1988). An evaluation of applied potential tomography in the diagnosis of infantile hypertrophic pyloric stenosis. *Clinical Physics and Physiological Measurement*, *9*(Suppl. A), 65–69.

Landweber, L. (1951). An iteration formula for Fredholm integral equations of the first kind. *Am. J. Math.*, *73*(3), 615–624. Au2

Leathard, A. D., Brown, B. H., Campbell, J. H., Zhang, F., Morice, A. H., & Tayler, D. (1994). A comparison of ventilatory and cardiac related changes in EIT images of normal human lungs and of lungs with pulmonary emboli. *Physiological Measurement*, *15*(Suppl. 2A), A137–A146.

Lionheart, W. R. B. (2004). EIT reconstruction algorithms: pitfalls, challenges and recent developments. *Physiological Measurement*, *25*(1), 125–142.

Liu, S., Fu, L., Yang, W. Q., Wang, H. G., & Jiang, F. (2004). Prior-online iteration for image reconstruction with electrical capacitance tomography. *IEE Proc. Sci. Meas. Technol.*, *151*(3), 195–200. Au2

Liu, S., Wang, H., Jiang, F., & Yang, W. Q. (2002). A new image reconstruction method for tomographic investigation of fluidized beds. *Am. Inst. Chem. Eng. J.*, *48*(8), 1631–1638.

Lux, H. D., Heinemann, U., & Dietzel, I. (1986). Ionic changes and alterations in the size of the extracellular space during epileptic activity. *Advances in Neurology*, *44*, 619–639.

Mangnall, Y. F., Baxter, A. J., Avill, R., Bird, N. C., Brown, B. H., Barber, D. C., Seagar, A. D., Johnson, A. G., & Read, N. W. (1987). Applied potential tomography: a new noninvasive technique for assessing gastric function. *Clinical Physics and Physiological Measurement*, *8* (Suppl. A), 119–129.

McAdams, E. T., McLaughlin, J. A., & McC Anderson, J. (1994). Multielectrode systems for electrical impedance tomography. *Physiological Measurement*, *15*(Suppl. 2A), A101–A106.

McArdle, F. J., Suggett, A. J., Brown, B. H., & Barber, D. C. (1988). An assessment of dynamic images by applied potential tomography for monitoring pulmonary perfusion. *Clinical Physics and Physiological Measurement*, *9*(Suppl. A), 87–91.

McArdle, F. J., Turley, A., Hussain, A., Hawley, K., & Brown, B. H. (1993). An in vivo examination of cardiac impedance changes imaged by cardiosynchronous averaging. In D. S. Holder (Ed.), *Clinical and Physiological Applications of Electrical Impedance Tomography* (pp. 257–268). London: UCL Press.

Metherall, P., Barber, D. C., Smallwood, R. H., & Brown, B. H. (1996). Three-dimensional electrical impedance tomography. *Nature*, *380*, 509–512.

Molinari, M., Cox, S. J., Blott, B. H., & Daniell, G. J. (2001a). Adaptive mesh refinement techniques for electrical impedance tomography. *Physiological Measurement*, *22*(1), 91–96.

Molinari, M., Cox, S. J., Blott, B. H., & Daniell, G. J. (2001b). Efficient non-linear 3D electrical tomography reconstruction. In *Proc. 2nd World Congress on Industrial Process Tomography* (pp. 424–432). August 29–31, Hannover, Germany.

Möller, P. H., Tranberg, K. G., Blad, B., Henriksson, P. H., Lindberg, L., Weber, L., et al. (1993). EIT for measurement of temperature distribution in laser thermotherapy (laserthermia). In D. S. Holder (Ed.), *Clinical and Physiological Applications of Electrical Impedance Tomography* (pp. 217–226). London: UCL Press.

Mueller, J. L., Isaacson, D., & Newell, J. C. (2001). Reconstruction of conductivity changes due to ventilation and perfusion from EIT data collected on a rectangular electrode array. *Physiological Measurement*, *22*(1), 97–106.

de Munck, J. C., Faes, T. J. C., & Heethaar, R. M. (1997). The use of the boundary element method in the forward problem of electrical impedance tomography. In *Proc. 19th Annu. Int. Conf. IEEE Eng. Med. Biol. Soc. (EMBS)* (pp. 445–448). October 30–November 2, Chicago, IL, USA.

Murphy, D., Burton, P., Coombs, R., Tarassenko, L., & Rolfe, P. (1987). Impedance imaging in the newborn. *Clinical Physics and Physiological Measurement*, *8*(Suppl. A), 131–140.

Nachman, A. I. (1995). Global uniqueness for a two-dimensional inverse boundary value problem. *Ann. Math.*, *142*, 71–96.

Newell, J. C., Edic, P. M., Xiaodan, R., Larson-Wiseman, J. L., & Danyleiko, M. D. (1996). Assessment of acute pulmonary edema in dogs by electrical impedance imaging. *IEEE Transactions on Biomedical Engineering*, *43*(2), 133–138.

Newell, J. C., Gisser, D. G., & Isaacson, D. (1988). An electric current tomograph. *IEEE Transactions on Biomedical Engineering*, *35*(10), 828–833.

Noble, T. J., Morice, A. H., Channer, K. S., Milnes, P., Harris, N. D., & Brown, B. H. (1999). Monitoring patients with left ventricular failure by electrical impedance tomography. *European Journal of Heart Failure*, *1*(4), 379–384.

Nopp, P., Harris, N. D., Zhao, T. X., & Brown, B. H. (1997). Model for the dielectric properties of human lung tissue against frequency and air content. *Medical and Biological Engineering and Computing*, *35*(6), 695–702.

Nour, S. (1992). *Measurement of gastric emptying in infants using APT*. Sheffield, UK: University of Sheffield Ph.D. thesis.

Ortega, J. M., & Rheinboldt, W. C. (1970). *Iterative Solution of Non-Linear Equations in Several Variables*. New York: Academic Press.

Osterman, K. S., Kerner, T. E., Williams, D. B., Hartov, A., Poplack, S. P., & Paulsen, K. D. (2000). Multifrequency electrical impedance imaging: preliminary in vivo experience in breast. *Physiological Measurement*, *21*(1), 99–109.

Osterman, K. S., Paulsen, K. D., & Hoopes, P. J. (1999). Application of linear circuit models to impedance spectra in irradiated muscle. *Annals of the New York Academy of Sciences*, *873*, 21–29.

Parker, R. L. (1984). The inverse problem of resistivity sounding. *Geophys.*, *49*(12), 2143–2158.

Patterson, R. P., & Zhang, J. (2003). Evaluation of an EIT reconstruction algorithm using finite difference human thorax models as phantoms. *Physiological Measurement*, *24*(2), 467–475.

Patterson, R. P., Zhang, J., Mason, L. I., & Jerosch-Herold, M. (2001). Variability in the cardiac EIT image as a function of electrode position, lung volume and body position. *Physiological Measurement*, *22*(1), 159–166.

Paulson, K., Lionheart, W., & Pidcock, M. (1993). Optimal experiments in electrical impedance tomography. *IEEE Transactions on Medical Imaging*, *12*(4), 681–686.

Pidcock, M. K., Kuzuoglu, M., & Leblebicioglu, K. (1995a). Analytic and semi-analytic solutions in electrical impedance tomography. I. Two-dimensional problems. *Physiological Measurement*, *16*(2), 77–90.

Pidcock, M. K., Kuzuoglu, M., & Leblebicioglu, K. (1995b). Analytic and semi-analytic solutions in electrical impedance tomography. II. Three-dimensional problems. *Physiological Measurement*, *16*(2), 91–110.

Ramirez, A., Daily, W., LaBrecque, D., Owen, E., & Chesnut, D. (1993). Monitoring an underground steam injection process using electrical resistance tomography. *Water Resources Research*, *29*(1), 73–87.

Ramirez, A. L., Daily, W. D., Binley, A. M., LaBrecque, D. J., & Roelant, D. (1996). Detection of leaks in underground storage tanks using electrical resistance methods. *J. Environ. Eng. Geophys.*, *1*(3), 189–203. Au2

Reigel, D. H., Dallman, D. E., Scarff, T. B., & Woodford, J. (1977). Transcephalic impedance measurement during infancy. *Developmental Medicine and Child Neurology*, *19*(3), 295–304.

Ritchie, I. K., Chesney, R. B., Gibson, P., Kulkarni, V., & Hutchison, J. M. (1989). Impedance osteography: a technique to study the electrical characteristics of fracture healing. *Biomedical Sciences Instrumentation*, *25*, 59–77.

dos Santos, C. C., & Slutsky, A. S. (2005). Novel advancements in the management and diagnosis of acute respiratory failure. In J. L. Vincent, A. Esteban, D. J. Cook & A. Anzueto (Eds.), *Evidence-Based Management of Patients with Respiratory Failure* (pp. 149–166). Berlin Heidelberg: Springer.

Santosa, F., & Vogelius, M. (1990). A backprojection algorithm for electrical impedance imaging. *SIAM J. Appl. Math.*, *50*(1), 216–243. Au2

Scharfetter, H., Merwa, R., & Pilz, K. (2005). A new type of gradiometer for the receiving circuit of magnetic induction tomography (MIT). *Physiological Measurement*, *26*(2), S307–S318.

Schuessler, T. F., & Bates, J. H. T. (1995). Utility of an esophageal reference electrode for thoracic electrical impedance tomography. In *Proc. 17th Annu. Int. Conf. IEEE Eng. Med. Biol. Soc. (EMBS)* (pp. 559–560). September 20–23, Montreal, Canada. Au2

Seagar, A. D., & Brown, B. H. (1987). Limitations in hardware design in impedance imaging. *Clinical Physics and Physiological Measurement*, *8*(Suppl. A), 85–90.

Seo, J. K., Pyo, H. C., Park, C., Kwon, O., & Woo, E. J. (2004). Image reconstruction of anisotropic conductivity tensor distribution in MREIT: computer simulation study. *Physics in Medicine and Biology*, *49*(18), 4371–4382.

Siltanen, S., Mueller, J., & Isaacson, D. (2000). An implementation of the reconstruction algorithm of A Nachman for the 2D inverse conductivity problem. *Inverse Problems*, *16* (3), 681–699.

Simske, S. (1987). *An adptive current determination and one-step reconstruction technique for a current tomography system*. Troy, NY, USA: Rensselaer Polytechnic Institute M.Sc. dissertation.

Smallwood, R. H., Mangnall, Y. F., & Leathard, A. D. (1994). Transport of gastric contents (electric impedance imaging). *Physiological Measurement*, *15*(Suppl. 2A), A175–A188.

Smallwood, R. H., Nour, S., Mangnall, Y. F., & Smythe, A. (1993). Impedance imaging and gastric motility. In D. S. Holder (Ed.), *Clinical and Physiological Applications of Electrical Impedance Tomography* (pp. 145–153). London: UCL Press.

Smulders, L. A. W., & van Oosterom, A. (1992). Application of electrical impedance tomography to the determination of lung volume. *Clinical Physics and Physiological Measurement*, *13*(Suppl. A), 167–170.

Somersalo, E., Cheney, M., & Isaacson, D. (1992). Existence and uniqueness for electrode models for electric current computed tomography. *SIAM J. Appl. Math.*, *52*(4), 1023–1040.

Somersalo, E., Cheney, M., Isaacson, D., & Isaacson, E. (1991). Layer stripping: a direct numerical method for impedance imaging. *Inverse Problems*, *7*(6), 899–926.

Soni, N. K., Paulsen, K. D., Dehghani, H., & Hartov, A. (2006). Finite element implementation of Maxwell's equations for image reconstruction in electrical impedance tomography. *IEEE Transactions on Medical Imaging*, *25*(1), 55–61.

Stefanesco, S., Schlumberger, C., & Schlumberger, M. (1930). Sur la distribution électrique potentielle autour d'une prise de terre ponctuelle dans un terrain à couchés horizontales, homogènes et isotropes. *Le Journal de Physique et le Radium*, *7*(1), 132–140.

Stuchly, M. A., & Stuchly, S. S. (1980). Dielectric properties of biological substances—tabulated. *The Journal of Microwave Power and Electromagnetic Energy*, *15*(1), 19–26.

Sutton, J. A., & McClelland, G. R. (1983). Epigastric impedance: a pharmacological test of a new non-invasive method of measuring the rate of gastric emptying. *British Journal of Anaesthesia*, *55*(9), 913.

Sylvester, J. (1992). A convergent layer stripping algorithm for the radially symmetric impedence tomography problem. *Commun. Part. Diff. Eq.*, *17*(11–12), 1955–1994.

Sylvester, J., & Uhlmann, G. (1986). A uniqueness theorem for an inverse boundary value problem in electrical prospection. *Commun. Pure Appl. Math.*, *39*(1), 91–112.

Szymanski, J. E., & Tsourlos, P. (1993). The resistive tomography technique for archaeology: an introduction and review. *Archaeologia Polona*, *31*, 5–32.

Tang, M., Wang, W., Wheeler, J., McCormick, M., & Dong, X. (2002). The number of electrodes and basis functions in EIT image reconstruction. *Physiological Measurement*, *23*(1), 129–140.

Tarantola, A., & Valette, B. (1982). Inverse problems = quest for information. *J. Geophys.*, *50*, 159–170.

Tarassenko, L., Murdoch, N., Rolfe, P., Weindling, A. M., & Costeloe, K. (1983). Cerebral electrical impedance measurements in the newborn. In *Proc. VIth Int. Conf. on Electrical Bio-impedance (ICEBI)* (pp. 166–170). September 12–14, Zadar, Yugoslavia.

Tarassenko, L., Pidcock, M. K., Murphy, D. F., & Rolfe, P. (1985). The development of impedance imaging techniques for use in the newborn at risk of intra-ventricular haemorrhage. In *Proc. Int. Conf. IEEE on Electric and Magnetic Fields in Medicine and Biol.* (pp. 83–87). December 4–5, London, UK.

Tarassenko, L., & Rolfe, P. (1984). Imaging spatial distributions of resistivity—an alternative approach. *Electronics Letters*, *20*(14), 574–576.

Thomas, D. C., McArdle, F. J., Rogers, V. E., Beard, R. W., & Brown, B. H. (1991). Local blood volume changes in women with pelvic congestion measured by applied potential tomography. *Clinical Science*, *81*(3), 401–404.

Tidswell, A. T., Gibson, A., Bayford, R. H., & Holder, D. S. (2001). Electrical impedance tomography of human brain activity with a two-dimansional ring of scalp electrodes. *Physiological Measurement*, *22*(1), 167–175.

Tidswell, T., Gibson, A., Bayford, R. H., & Holder, D. S. (2001). Three-dimensional electrical impedance tomography of human brain activity. *NeuroImage*, *13*(2), 283–294.

Tikhonov, A. N., & Arsenin, V. Y. (1977). *Solution of Ill-Posed Problems*. New York: Wiley.

Tizzard, A., Horesh, L., Yerworth, R. J., Holder, D. S., & Bayford, R. H. (2005). Generating accurate finite element meshes for the forward model of the human head in EIT. *Physiological Measurement*, *26*(2), S251–S261.

Toft, P. (1996). *The Radon transform—theory and implementation*. Copenhagen, Denmark: Technical University of Denmark Ph.D. thesis.

Tong, P., & Rossettos, J. N. (1977). *Finite-Element Method: Basic Technique and Implementation*. Cambridge, MA, USA: MIT Press.

Trokhanova, O., Karpov, A., Cherepenin, V., Korjenevsky, A., Kornienko, V., Kultiasov, Y., et al. (2001). Electro-impedance mammography testing at some physiological woman's periods. In *Proc. XIth Int. Conf. on Electrical Bio-impedance (ICEBI)* (pp. 461–465). June 17–21, Oslo, Norway.

Ultchin, Y., Nachaliel, U., & Ori, A. (2002). Indirect calculation of breast tissue impedance values. *Physiological Measurement*, *23*(1), 177–182.

Vaisman, N., Weintrop, N., Blumental, A., Yosefsberg, Z., & Vardi, P. (1999). Gastric emptying in patients with type I diabetes mellitus. *Annals of the New York Academy of Sciences*, *873*, 506–511.

Van Harreveld, A., & Ochs, S. (1956). Cerebral impedance changes after circulatory arrest. *American Journal of Physiology*, *187*(1), 180–192.

Van Harreveld, A., & Schadé, J. P. (1962). Changes in the electrical conductivity of cerebral cortex during seizure activity. *Experimental Neurology*, *5*(5), 383–400.

Vauhkonen, M., Kaipio, J. P., Somersalo, E., & Karjalainen, P. A. (1997). Electrical impedance tomography with basis constraints. *Inverse Problems*, *13*(2), 523–530.

Vauhkonen, M., Vadasz, D., Karjalainen, P. A., Somersalo, E., & Kaipio, J. P. (1998). Tikhonov regularization and prior information in electrical impedance tomography. *IEEE Transactions on Medical Imaging*, *17*(2), 285–293.

Vauhkonen, P. J., Vauhkonen, M., Savolainen, T., & Kaipio, J. P. (1999). Three-dimensional electrical impedance tomography based on the complete electrode method. *IEEE Transactions on Biomedical Engineering*, *46*(9), 1150–1160.

Wang, H., Wang, C., & Yin, W. (2004). A pre-iteration method for the inverse problem in electrical impedance tomography. *IEEE Trans. Instrum. Meas.*, *53*(4), 1093–1096.

Wang, J. Z., Williamson, S. J., & Kaufman, L. (1992). Magnetic source images determined by a lead-field analysis: the unique minimum-norm least-squares estimation. *IEEE Transactions on Biomedical Engineering*, *39*(7), 665–675.

Watson, S. J., Smallwood, R. H., Brown, B. H., Cherian, P., & Bardhan, K. D. (1996). Determination of the relationship between the pH and conductivity of gastric juice. *Physiological Measurement*, *17*(1), 21–27.

Williams, R. A., & Beck, M. S. (1995). *Process Tomography: Principles, Techniques and Applications*. Oxford, UK: Butterworth-Heinemann.

Witsoe, D. A., & Kinnen, E. (1967). Electrical resistivity of lung at 100 kHz. *Medical and Biological Engineering and Computing*, *5*(3), 239–248.

Woo, E. J., Webster, J. G., & Tompkins, W. J. (1990). The improved Newton Raphson method and its parallel implementation for static impedance imaging. In *Proc. 12th Annu. Int. Conf. IEEE Eng. Med. Biol. Soc. (EMBS)* (pp. 102–103). November 1–4, Philadelphia, PA, USA. Au2

Wright, J. W., & Evans, D. F. (1990). Applied potential tomography (APT): a non-invasive method of detecting the migrating motor complex (MMC). In T. J. Hames (Ed.), *Proc. of the*

Copenhagen Meeting on Electrical Impedance Tomography (pp. 270–275). Sheffield, UK: Sheffield University.

Xie, C. G., Huang, S. M., Hoyle, B. S., & Beck, M. S. (1991). Tomographic imaging of industrial process equipment—development of system model and image reconstruction algorithm for capacitive tomography. In *Proc. Vth IOP Conf. on Sensors and Their Applications* (pp. 203–208). September 22–25, Edinburgh, Scotland.

Xu, P. (1998). Truncated SVD methods for discrete linear ill-posed problems. *Geophys. J. Int.*, *135*(2), 505–514. Au2

Yang, W. Q., Stott, A. L., Beck, M. S., & Xie, C. G. (1995). Development of capacitance tomographic imaging systems for oil pipeline measurements. *Review of Scientific Instruments*, *66*(8), 4326–4332.

Yorkey, T. J. (1990). Electrical impedance tomography with piecewise polynomial conductivities. *Journal of Computational Physics*, *91*(2), 344–360.

Yorkey, T. J., Webster, J. G., & Tompkins, W. J. (1987). Comparing reconstruction algorithms for electrical impedance tomography. *IEEE Transactions on Biomedical Engineering*, *34*(11), 843–852.

Comp. by: pg1384Alex, Monica Stage: Proof ChapterID: 0001157249AIEP978-0-12-381316-9 Date:22/4/10 Time:12:24:34
File Path:\\pchns1002z\WOMAT\Production\PRODENV\0000000001\0000018453\0000000016\0001157249.3d
Acronym:AIEP Volume:16204

Author Query Form

Book Series: Advances in Imaging and Electron Physics 162
Chapter 04

ELSEVIER

Dear Author,

During the preparation of your manuscript for typesetting some questions have arisen. These are listed below. Please check your typeset proof carefully and mark any corrections in the margin of the proof or compile them as a separate list. This form should then be returned with your marked proof/list of corrections to Elsevier Science.

Disk use

In some instances we may be unable to process the electronic file of your article and/or artwork. In that case we have, for efficiency reasons, proceeded by using the hard copy of your manuscript. If this is the case the reasons are indicated below:

☐ Disk damaged ☐ Incompatible file format ☐ LaTeX file for non-LaTeX journal

☐ Virus infected ☐ Discrepancies between electronic file and (peer-reviewed, therefore definitive) hard copy.

☐ Other: ....

We have proceeded as follows:

☐ Manuscript scanned ☐ Manuscript keyed in ☐ Artwork scanned

☐ Files only partly used (parts processed differently:..)

Bibliography

If discrepancies were noted between the literature list and the text references, the following may apply:

☐ The references listed below were noted in the text but appear to be missing from your literature list. Please complete the list or remove the references from the text.

☐ Uncited references: This section comprises references which occur in the reference list but not in the body of the text. Please position each reference in the text or, alternatively, delete it. Any reference not dealt with will be retained in this section.

Query Refs.	Details Required	Author's response
AU1	This reference not cited in the text part	
AU2	Please provide expansion for the journal title.	
AU3	Please check the running head.	